The UKIRT Infrared Deep Sky Survey Early Data Release

S. Dye[1]⋆, S. J. Warren[2], N. C. Hambly[3], N. J. G. Cross[3], S. T. Hodgkin[4],
M. J. Irwin[4], A. Lawrence[3], A. J. Adamson[5], O. Almaini[6], A. C. Edge[7],
P. Hirst[5], R. F. Jameson[8], P. W. Lucas[9], C. van Breukelen[10], J. Bryant[3],
M. Casali[11], R. S. Collins[3], G. B. Dalton[10], J. I. Davies[1], C. J. Davis[5],
J. P. Emerson[12], D. W. Evans[4], S. Foucaud[6], E. A. Gonzales-Solares[4],
P. C. Hewett[4], T. R. Kendall[9], T. H. Kerr[5], S. K. Leggett[5], N. Lodieu[8],
J. Loveday[13], J. R. Lewis[4], R. G. Mann[3], R. G. McMahon[4], D. J. Mortlock[2],
Y. Nakajima[14], D. J. Pinfield[9], M. G. Rawlings[5], M. A. Read[3], M. Riello[4],
K. Sekiguchi[15], A. J. Smith[13], E. T. W. Sutorius[3], W. Varricatt[5], N. A. Walton[4],
S. J. Weatherley[16]

[1] *Cardiff University, School of Physics & Astronomy, Queens Buildings, The Parade, Cardiff, CF24 3AA, U.K.*
[2] *Astrophysics Group, Imperial College London, Blackett Laboratory, Prince Consort Road, London, SW7 2AZ, U.K.*
[3] *Royal Observatory Edinburgh, Blackford Hill, Edinburgh, EH9 3HJ, U.K.*
[4] *Institute of Astronomy, Madingley Rd., Cambridge, CB3 0HA, U.K.*
[5] *Joint Astronomy Centre, 660 N. A'ohoku Place, University Park, Hilo, Hawaii 96720, U.S.A.*
[6] *School of Physics and Astronomy, University of Nottingham, University Park, Nottingham, NG7 2RD, U.K.*
[7] *Department of Physics, Durham University, South Road, DH1 3LE, U.K.*
[8] *Department of Physics and Astronomy, University of Leicester, Leicester, LE1 7RH, U.K.*
[9] *Centre for Astrophysics Research, Science and Technology Research Institute, University of Hertfordshire, Hatfield, AL10 9AB, U.K.*
[10] *Department of Physics, Denys Wilkinson Building, Keble Road, Oxford, OX1 3RH, U.K.*
[11] *ESO, Karl-Schwarzschild-Str. 2, D-85748 Garching bei München, Germany*
[12] *Astronomy Unit, School of Mathematical Sciences, Queen Mary, University of London, Mile End Road, London E1 4NS*
[13] *Department of Physics and Astronomy, University of Sussex, Brighton, East Sussex, BN1 9QH, U.K.*
[14] *National Astronomical Observatory of Japan, 2-21-1 Osawa, Mitaka, Tokyo, 181-8588, JAPAN*
[15] *Subaru Telescope, National Astronomical Observatory of Japan, 650 North A'ohoku Place, Hilo, HI 96720, U.S.A.*
[16] *Detica, Surrey Research Park, Guildford, Surrey, GU2 7YP, U.K.*

Document in prep.

ABSTRACT

This paper defines the UKIRT Infrared Deep Sky Survey (UKIDSS) Early Data Release (EDR). UKIDSS is a set of five large near-infra-red surveys defined by Lawrence et al. (2006), being undertaken with the UK Infra-red Telescope (UKIRT) Wide Field Camera (WFCAM). The programme began in May 2005 and has an expected duration of seven years. Each survey uses some or all of the broadband filter complement $ZYJHK$. The EDR is the first public release of data to the European Southern Observatory (ESO) community. All worldwide releases occur after a delay of 18 months from the ESO release. The EDR provides a small sample dataset, ~ 50 deg^2 (about 1% of the whole of UKIDSS), that is a lower limit to the expected quality of future survey data releases. In addition, an EDR+ dataset contains all EDR data plus extra data of similar quality, but for areas not observed in all of the required filters (amounting to ~ 220 deg^2). The first large data release, DR1, will occur in mid-2006. We provide details of the observational implementation, the data reduction, the astrometric and photometric calibration, and the quality control procedures. We summarise the data coverage and quality (seeing, ellipticity, photometricity, depth) for each survey and give a brief guide to accessing the images and catalogues from the WFCAM Science Archive.

Key words: astronomical data bases: surveys – infrared: general

arXiv:astro-ph/0603608v2 1 Sep 2006

1 INTRODUCTION

UKIDSS is the UKIRT Infrared Deep Sky Survey (Lawrence et al. 2006), carried out using the Wide Field Camera (WFCAM; Casali et al. 2006) installed on the United Kingdom Infrared Telescope (UKIRT). Survey data acquisition started in May 2005. This paper defines the UKIDSS Early Data Release (EDR), the first release of UKIDSS data products to the ESO-wide astronomical community. The data were released on 10th February 2006, and are available from http://surveys.roe.ac.uk/wsa.

UKIDSS is a programme of five individual surveys that each use some or all of the broadband filter complement $ZYJHK$ (described by Hewett et al. 2006), and that span a range of areas and depths. There are three high galactic latitude surveys; the Large Area Survey (LAS), the Deep Extra-galactic Survey (DXS), and the Ultra Deep Survey (UDS), covering complementary combinations of area and depth. Besides the LAS, there are two other wide surveys at low galactic latitudes, aimed at targets in the Milky Way; the Galactic Plane Survey (GPS), and the Galactic Clusters Survey (GCS). The three wide, shallow surveys, LAS, GCS and GPS, use a total integration time of 40s or 80s per field per filter. The layout and filter complement of each survey are provided in Section 4. The complete UKIDSS programme is scheduled to take 7 years, requiring ∼1000 nights on UKIRT. The course of the full 7 year programme will be guided, to a certain extent, by the progress and scientific findings of the first two years of surveying. The design of these first two years consists of a set of fixed, shorter-term goals that define the '2–year plan'.

The purpose of the present paper is to provide a self–contained guide to the EDR. We have therefore included relevant background information extracted from the set of UKIDSS reference technical papers on; the surveys (Lawrence et al. 2006), the photometric system (Hewett et al. 2006), the camera (Casali et al. 2006), the data pipeline (Irwin et al. 2006), and the data archive (Hambly et al. 2006), compressing details that will be the same for all data releases, and expanding on details that are specific to the EDR. The name EDR is copied from the Sloan Digital Sky Survey (SDSS) EDR (Stoughton et al. 2002) since the UKIDSS EDR serves a similar purpose to the SDSS EDR, i.e. it is a prototype of future larger releases. Similarly, the introduction to UKIDSS given by Lawrence et al. (2006) mirrors the purpose of York et al. (2000), introducing SDSS. We will also follow SDSS by naming the first large data release 'DR1'. The SDSS and 2 Micron All Sky Survey (2MASS; Skrutskie et al. 2006) have both fundamentally influenced the design of all elements of UKIDSS.

The outline of the paper is as follows: In the next section, we discuss the background to the UKIDSS programme. In Section 3, we provide a brief description of WFCAM, and in Section 4 we give an overview of the UKIDSS 2-year goals, in terms of area and filter coverage for each survey. We then follow the data-train sequence. In Section 5 we provide details of the observational implementation of the surveys, at a level that is required for understanding the data. For example, this includes offsetting, microstepping and stacking (i.e. averaging) strategies which dictate the structure of the image files. Section 6 describes the data reduction pipeline, and the procedures followed for the astrometric and pho-

tometric calibration of the data. Section 7 catalogues a variety of artifacts that can occur in the data. The output from the pipeline is a set of reduced, stacked frames and associated catalogues of detected objects. After ingestion to the archive, an initial series of quality control (QC) tests reject sub-standard data before the catalogues across different bands are merged. A second round of QC checks are then applied to the merged catalogues. Section 8 describes these QC procedures. The contents of the EDR are described in Section 9, where, in particular, plots of the distribution of the fields on the sky are provided. Access to the EDR is through the WFCAM Science Archive (WSA), which is described in Section 10.

2 UKIDSS BACKGROUND

The design and implementation of the UKIDSS programme is the responsibility of the UKIDSS Consortium, an assemblage of astronomers with a common aim of completing the surveys. Observing is shared between UKIRT staff and UKIDSS astronomers. UKIDSS is an ESO public survey and UKIDSS consortium members have no proprietary data rights. Acquired data are shipped from UKIRT to the Cambridge Astronomical Survey Unit (CASU) at weekly intervals. At this stage, a copy of the raw UKIDSS data is sent from CASU to the ESO archive. At CASU, the data are processed by the WFCAM pipeline to produce stacked image data and source catalogues (see Section 6). The processed data products are electronically transferred to the Wide Field Astronomical Unit (WFAU) in Edinburgh where they are ingested by the WSA (see Section 10). All WFCAM data, whether UKIDSS or not, follows the same route. UKIDSS, being the largest WFCAM user, has interacted closely on the design and development of the pipeline and archive.

Following commissioning of WFCAM, a few nights (approximately 10 hours per survey) were devoted to science verification (SV) observations, in order to test the entire data train made up of the three elements: 1) the observational strategies employed by the different surveys (e.g. to check that integration times give background limited observations, offset patterns enable good sky correction and guide stars are sufficiently bright), 2) the processing steps executed by the WFCAM pipeline, from flatfielding and sky correction of the image data, to stacking and catalogue generation, 3) the functionality of the WSA, both archive ingest and source merging, and retrieval of the image and catalogue data through the web-based user interface (see Section 10). The SV data were analysed by UKIDSS consortium members, the results were fed back to CASU and WFAU, and the process was repeated after adjustments to the pipeline and archive. On the basis of the SV results, a set of QC procedures for UKIDSS data was agreed (described in Section 8) and then applied to the EDR by WFAU. The SV dataset, much smaller than the EDR, is mostly heterogeneous. With the exception of some DXS data, the SV data have not been included in the EDR.

WFCAM is scheduled in blocks, a few months at a time, separated by intervals of a few months, and in such a way as to ensure that over a two-year span, access over the entire RA range is reasonably uniform. UKIDSS uses about

40% of all UKIRT time. The first WFCAM survey block, hereafter 05A, included UKIDSS survey observations over several nights commencing 13th May and ending 19th June 2005. All data from 05A that passes QC is released here. Additionally some DXS data taken in the science verification phase, back to 9th April have been included. The second block, hereafter 05B, commenced 27th Aug 2005 and ended 25th January 2006. DXS and UDS data taken in 05B up to 27th September 2005, that satisfy QC, are also included in this release. Some changes to observing procedures, detailed in Section 5, were made between semesters 05A and 05B. Further changes are not anticipated.

The 05A data are somewhat inferior to the 05B data in terms of image quality and cosmetics. Correct alignment of the instrument requires that the instrument focal plane assembly and optical focal plane be co-planar to within a small fraction of a milliradian. This can only be measured on sky, but requires disassembly of the instrument to adjust properly. An interim adjustment can be made by tilting the secondary mirror of the telescope as this results in a corresponding tilt of the optical focal plane, though this introduces other aberrations into the optics. The 05A data were taken with this type of interim adjustment in place and in good seeing it is evident that the data are compromised by this. The instrument was opened up and the alignment corrected internally between the 05A and 05B observing blocks. Secondly, there is an issue of out–of–focus images of dirt on the field lens (see Section 7), which forms the end of the barrel of the instrument. Because the lens lies close to an intermediate focus, out–of–focus images of dust or marks on the lens are visible in some frames. The top surface is frequently cleaned, while the bottom surface was cleaned in the interval between the 05A and 05B blocks to remove marks left by a lens handling jig, visible in the 05A data.

The EDR dataset is relatively large compared to existing near-infra-red surveys (about as many photons have been collected as in 2MASS), and will be useful for science exploitation. However, compared to the whole of UKIDSS the EDR is only a small fraction, about 1%. From the UKIDSS perspective, the EDR is therefore a small prototype sample, released to the community as a stepping stone toward the goal of routine and prompt release of survey-quality data. We welcome feedback on the quality of the data and the functionality of the WSA. We aim to finalise the details of the data-train that define survey-quality products over early 2006, with further refinements of the pipeline, as well as adjustments and additions to the QC procedures. The entire 05A and 05B data will then be prepared for the first large data release, DR1, scheduled for mid-2006. With this in mind, and considering the image quality and cosmetic issues of the 05A data, we have relaxed the QC criteria to a limited extent (e.g. depth and seeing), with the consequence that some fields included in the EDR will be excluded from DR1 and instead will be re-observed.

The EDR appears in the WSA as two databases. The EDR database is all the data where, for any pointing, the images and catalogues in all filters for that survey are available and pass QC. The EDR+ database is all of the EDR data plus the remainder that passes QC, i.e. pointings where the full complement of filters for that survey is incomplete, either because some remain to be observed, or because some failed QC. In the remainder of the paper, where it is appropri-

ate to make the distinction, we refer to the 'EDR database' and the 'EDR+ database'. The general term 'EDR' implies the combination. The extra content of the EDR+ database is very heterogeneous in terms of completeness of the filter complement so that its usefulness is less apparent, considering that the surveys were designed around science goals that require the complete filter complement. We therefore anticipate that users will be most interested in the EDR database. Accessing the two databases is explained in detail in Section 10.

The first UKIDSS observations were made in May 2005, so that EDR represents a maximum lag of 9 months from acquisition to release. After finalisation of the pipeline and QC procedures, and automation of the latter, the time-lag will rapidly diminish. At present the policy is that a release will occur once all data from an observing block have been processed. Ideally the delay from completion of the observing block to release of the data will become as short as 3 months. Each release will be accompanied by an announcement publication defining the specific data products included in that release.

3 WFCAM

WFCAM was built by the UK Astronomical Technology Centre (UK ATC) in Edinburgh as a common user instrument for UKIRT. The UKIDSS programme owes its feasibility to the large field of view of the camera. This section provides details of the design and construction of WFCAM, relevant for understanding the contents of the EDR, including some of the unusual properties of WFCAM data, as well as the characteristics peculiar to this release. We refer the reader to Casali et al. (2006) for full technical details of WFCAM.

The survey speed of an instrument is proportional to the telescope+instrument étendue[1]. At the time of writing, WFCAM's étendue of $2.38 \, \text{m}^2 \, \text{deg}^2$ is the largest of any near-infrared imager in the world. The large field of view of WFCAM, $0.21 \, \text{deg}^2$, is achieved with four Rockwell Hawaii-II 2048×2048 18μm-pixel array detectors, with a relatively large pixel scale of $0.4''$. In good seeing the point spread function (PSF) is consequently under-sampled. Microstepping and interlacing allow sampling on scales of $1/2$ or $1/3$ of a pixel (see Section 5). The layout of the four detectors and their numbering scheme is shown in Figure 1. The detectors cannot be butted because of their packaging. Instead they are spaced at 94% of the detector width, as shown. Four exposures are required to survey a contiguous area, referred to as a 'Tile' (see Section 5.1). As indicated in Figure 1, each detector is rotated by 90° with respect to its neighbours. The pixel x, y coordinate convention is indicated for the detectors.

Each detector is divided into quadrants, and each quadrant is divided into eight channels of 128×1024 pixels. The channel packing relative to the xy axes is illustrated in Figure 1. The packing rotates through 90° in moving to an adjacent quadrant. This channel packing arrangement is visible for detector 4 in Figure 3.

---

[1] product of telescope collecting area, and solid angle of instrument field of view, sometimes called *grasp*
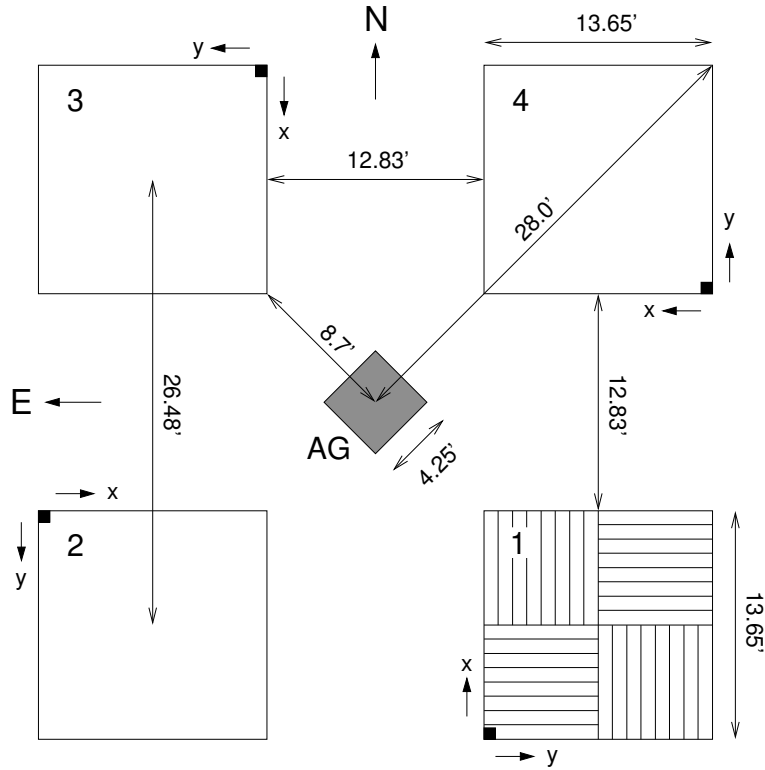
Figure 1. Layout of the WFCAM focal plane. Detector numbering follows that used in the WSA and is the same as the extension numbering in the FITS data files. Detectors are divided into four quadrants, each quadrant having 8 channels as illustrated in detector 1. The autoguider (grey shading) sits at the centre of the focal plane. North is up, East is left.

The optical path is illustrated in Casali et al. (2006). The design involves a new $f/9$ secondary, which produces an intermediate focus 5.7m above the primary. A tertiary mirror returns the beam upward to the downward–looking focal plane. For the purposes of this paper, an important element of the design is a field lens, which gives rise to two types of artifact in the data (Section 7). The field lens images the primary mirror to a cold stop inside the cryostat, which baffles stray thermal emission. The lens lies near the intermediate focus, and forms the end of the barrel of the instrument. There is an auxiliary lens mounted at the centre and just above the field lens. The purpose of the auxiliary lens is to raise the autoguider focal plane, and to change the f-ratio to achieve the required pixel scale. The autoguider is located on the optical axis, as shown. It was necessary to raise the guider CCD above the focal plane because of the packaging of the Hawaii-II detectors.

WFCAM has eight filter housings. Because the focal plane vignettes the beam, to minimise throughput loss the filters are stored vertically, rather than in a wheel. Consequently the detectors are exposed to unfiltered light when the filter is changed. Currently, the standard filter complement includes the broadband set $ZYJHK$, and two narrow-band filters, H_2 1-0 S1 & Brγ. The eighth filter housing is blanked for darks. The WFCAM J, H and K band-passes follow the specification of the Mauna Kea filter set (Tokunaga, Simons & Vacca 2002). The WFCAM Z filter has an effective wavelength of 0.87μm and the WFCAM Y filter fills the gap between Z and J. The system throughput, above-atmosphere-to-detector, is close to 20% at J, slightly

higher at H and K, and slightly lower at Z and Y. The $ZYJHK$ photometric system of the instrument has been characterised by Hewett et al. (2006), who provide the total system response curves for each broad band, as well as colour equations to translate to 2MASS JHK (see also Section 6.4) and SDSS z, and synthetic colours of a wide variety of stars, galaxies and quasars.

UKIDSS observations are made in one of two read modes. In correlated double sampling (CDS), after a detector reset, an initial read is made, followed by an exposure of the desired length, followed by a final read. The resulting output is the difference of the two reads. In non-destructive read (NDR) mode, after the detector reset, several reads sample the build up of charge throughout the exposure, and the counts are established by a linear fit. CDS has higher read-noise $\sim 30e^-$, but the likelihood of electronic pick-up due to the reduced read activity is smaller than with NDR. CDS is used for all UKIDSS JHK observations, which use shorter integrations because of the high background. NDR has lower read-noise $\sim 20e^-$, but is affected more by amplifier glow (although at present, this is well removed by dark subtraction). Also, although measurements currently indicate that detector responses are linear (Irwin et al. 2006), if the need for linearisation should arise in the future, then this correction is a more challenging computational problem than with CDS. NDR is used for all ZY observations, which use longer exposures, to achieve sky-noise limited performance.

The detectors are of PACE manufacture. The frames exhibit four characteristics that are unwelcome: pixel covari-

ance, curtaining, persistence, and cross-talk. *Pixel covariance* is a result of inter-pixel capacitance. The result is that the pixel to pixel variance is reduced by a factor of about 1.2, and that the readout gain (photons per ADU) is overestimated by this factor when computed in the traditional way using photon–noise transfer curves. In this paper, where appropriate, e.g. in computing the system throughput, we have compensated for the effect. *Curtaining* is a rapidly varying constant bias offset along each 'line', where the pattern repeats in each quadrant (rotating in the same manner as the channel packing). The term 'line' here means 1024 pixels along the direction of the short axis of the channels. The pattern fluctuates with a root mean square (RMS) of $10e^-$ to $15e^-$ and is completely random; no two detector frames are ever affected in the same way. *Persistence* is the effect of image latency whereby counts from a bright source are not completely removed after a detector reset. Artificial images of sources can also occur due to *cross-talk* between the detector channels within a quadrant. Persistence and cross-talk are described in Section 6 and all effects are discussed at greater length by Irwin et al. (2006).

4   THE UKIDSS 2-YEAR PLAN

The design and layout of the surveys are set out in Lawrence et al. (2006) which is the reference work for details of the final (7-year) goals of the UKIDSS programme. These goals are summarised in Table 1 in terms of areas, filters, number of passes, and (final summed) depth. All depths quoted in this paper are in the Vega photometric system and correspond to the total brightness of a point source for which the summed flux in a $2''$ diameter aperture has, on average, S/N=5. The original designed depths were based on a first estimate of sensitivities in each band, made in 2001 and later revised brighter. It is apparent from analysis of the EDR dataset that the achieved sensitivities are indeed shallower than the original estimates, by an average of 0.2 mag. In light of this, all target depths have been adjusted by 0.2 mag and these are the values quoted here and in Lawrence et al. (2006). The overestimate of the detector quantum efficiency, due to pixel covariance (Section 3), is the main contribution to the overestimate of the instrument throughput.

In each of the shallow surveys, the depth in a select filter (J for LAS, K for GCS, GPS) is built up in two or three passes, in order to provide proper motions and variability information. Thus any field is observed in the full filter complement at one epoch and observed in the select filter only at one or two other epochs. The repeat passes are separated by a minimum of two years, to provide a sufficient baseline for measurement of proper motions. For scheduling reasons, in some areas the first epoch is with the full filter complement, and in other areas the first epoch is with the select filter.

The surveys are currently focused on completing a set of goals for the first two years of operations, hereafter referred to as the 2-year plan. In this section we describe the 2-year plan, which provides the context of the EDR and explains, for example, why some areas are covered in only a single band. In the 2-year plan the LAS and GCS are accelerated relative to the other surveys.

Survey	Area (deg^2)	Filter	No. passes	Depth
LAS	4028	Y	1	20.3
		J	2	19.9
		H	1	18.6
		K	1	18.2
GPS	1868	J	1	19.9
	1868	H	1	19.0
	1868	K	3	19.0
	300	H_2	3	...
GCS	1067	Z	1	20.4
		Y	1	20.3
		J	1	19.5
		H	1	18.6
		K	2	18.6
DXS	35	J	multiple	22.3
	5	H	multiple	21.8
	35	K	multiple	20.8
UDS	0.77	J	multiple	24.8
		H	multiple	23.8
		K	multiple	22.8

Table 1. Summary of the final (7-year) goals of the UKIDSS programme. Depth is in the Vega system and corresponds to the total brightness of a point source for which the flux in a $2''$ diameter aperture has S/N=5. The GPS depths refer to uncrowded fields.

Table 2 summarises the relevant details of the 2-year plan for each survey, listing area to be surveyed, filter, target depth and default integration time, for the shallow surveys, for good conditions. As explained in Section 5, in cases of mediocre seeing, bright sky or thin cirrus, observations in some fields are still undertaken, but the integration times are increased to ensure the target depth is achieved. The geometry of the target areas in the 2-year plan is shown in Figure 2. In what follows, we provide additional details of the 2-year plan, describing each survey in turn. Section 9 describes the data content of the EDR.

4.1   LAS 2-year plan

The LAS is made up of 3 blocks, visible in Figure 2. All three blocks lie within the SDSS footprint. In the southern galactic hemisphere there is an equatorial stripe, Block 1, of area 212 deg^2. In the northern galactic hemisphere, there is an equatorial block, Block 2, and a block at higher declinations, Block 3, both of area 1908 deg^2. The LAS 2-year plan is to survey Block 1 and Block 2 in a single pass in $YJHK$. In addition, depending on conditions (Section 5), part of Block 3, an estimated 1000 deg^2, will be covered in a single pass in J only. For scheduling purposes each block has been subdivided into regions. The EDR contains data from the regions marked LAS1, LAS2, LAS3 & LAS4 (see Section 9).

4.2   GPS 2-year plan

The GPS will cover the band of galactic latitude $|b| < 5°$, that lies within the declination range $-20° < \delta < +60°$. This translates to two blocks defined by the galactic longitude ranges $15° < l < 107°$ and $142° < l < 230°$. In addi-
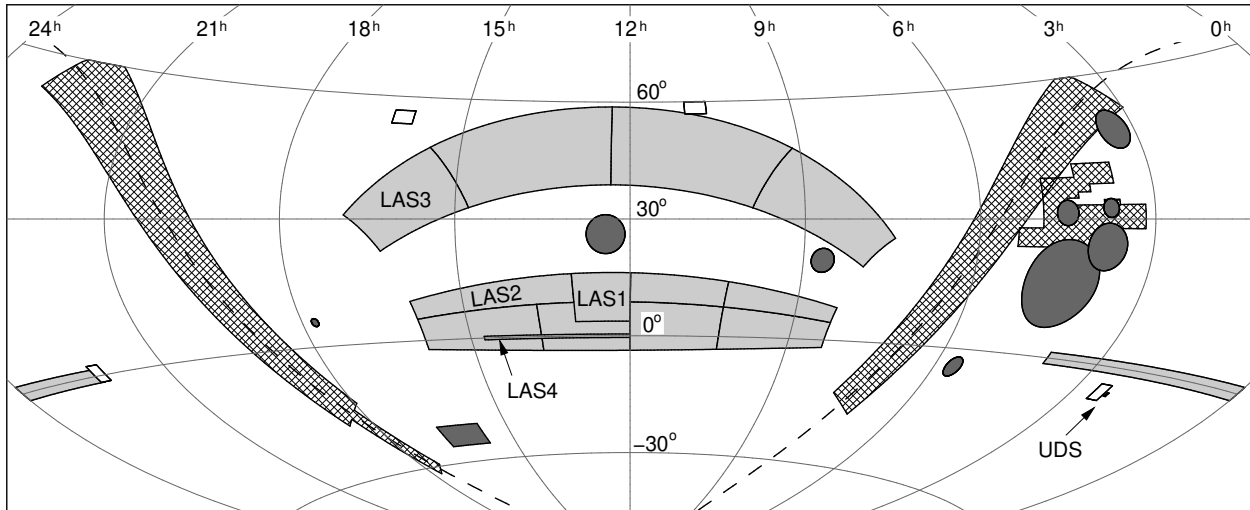
Figure 2. The UKIDSS 2 year plan survey areas showing the LAS (solid light grey), GPS (cross-hatched), GCS (solid dark grey), DXS (empty squares) and UDS (as labelled, lying alongside the western-most DXS field). The dashed line indicates the galactic plane. The LAS is shown here divided into its constituent projects (see Section 5.1), the EDR containing data in LAS1-4. Note that in the 2-year plan the LAS northern block receives J only coverage and most of the GPS areas shown receive K only (see text).

Survey	Area (deg^2)	Filter	Depth	t_{int}
LAS	2120	Y	20.3	40s
	3120	J	19.5	40s
	2120	H	18.6	40s
	2120	K	18.2	40s
GPS	338	J	19.9	80s
	338	H	19.0	80s
	1868	K	18.2	40s
	300	H_2	...	150s
GCS	237	Z	20.4	40s
	237	Y	20.3	40s
	237	J	19.5	40s
	237	H	18.6	40s
	606	K	18.2	40s
DXS	12.6	J	22.3	
	12.6	K	20.8	
UDS	0.77	J	23.8	
	0.77	K	22.8	

Table 2. Summary of the goals of the UKIDSS 2-year plan. Depth is in the Vega system and corresponds to the total brightness of a point source for which the flux in a $2''$ diameter aperture has S/N=5. The GPS depths refer to uncrowded fields. For the shallow surveys the default integration time for normal conditions is listed. Some fields are observed in mediocre conditions, with longer integration times, as detailed in Section 5.

tion, there will be a thin extension into the galactic Centre, defined by $|b| < 2°$, $-2° < l < 15°$, as well as imaging of the ~ 300 deg^2 Taurus-Auriga-Perseus star-formation complex. The geometry of Taurus-Auriga-Perseus is shown by the irregular cross-hatched area in Figure 2 which follows the CO gas map of Ungerechts & Thaddeus (1987)

The fields for the first two years will concentrate on the region of the inner Galaxy, close to the plane. The region $|b| < 1°$ in the longitude range $-2° < l < 107°$ will

be imaged in JHK. This includes the area covered by the northern half of the GLIMPSE survey (Churchwell et al. 2002) using the Spitzer Space Telescope. Also, the block covering $30° < l < 45°$ will be imaged in JHK, over the remainder of the full thickness, $|b| < 5°$. The whole of the remainder of the GPS area will be surveyed in K only, excluding Taurus-Auriga-Perseus which will be imaged in $H_2 + JHK$ in clear weather, or $H_2 + K$ in thin cirrus conditions. This ensures a 2 year baseline between $H_2 + K$ observations (at least) of the complex over the full 7 year plan. For more information and details of updates, we refer the reader to the GPS web site located at *http://star-www.herts.ac.uk/~pwl/UKIDSS_GPS.html*.

4.3 GCS 2-year plan

The GCS will observe the 10 star clusters listed in Table 3. These are ranked by priority, which gives an indication of the sequence in which they will be completed. In the 2-year plan, five of the clusters will be completed in all filters, as well as the central regions of three other clusters, as listed in the table. In addition, the two remaining clusters will be covered in K only.

For the GCS, the EDR contains data from the Sco and Coma-Ber clusters. For more information and details of updates, we refer the reader to the GCS web site located at *http://www.roe.ac.uk/~nch/gcs/*.

4.4 DXS 2-year plan

The DXS comprises 12 contiguous Tiles in each of four fields; XMM-LSS (2^h25^m,$-4°30'$), ELAIS N1 (16^h10^m,$+54°00'$), the Lockman Hole (10^h57^m,$+57°40'$) and VIMOS 4 (22^h17^m,$+0°20'$). The 2-year plan is to reach full depth in four Tiles in J and K in each of the four fields. Rather than build up depth over all four Tiles, the strategy is to achieve target depth in one Tile before moving on to the next.

Field	Type	RA, Dec	Filters	Area (deg^2)
IC 4665	OC	17:46,+05:43	$ZYJHK$	3.1
Pleiades	OC	03:47,+24:07	$ZYJHK$	79
Alpha Per	OC	03:22,+48:37	$ZYJHK$	50
Praesepe	OC	08:40,+19:40	$ZYJHK$	28
Tau.-Aur.	SFA	04:30,+25:00	$ZYJHK$	cen. 24
Orion	SFA	05:29,−02:36	$ZYJHK$	cen. 16
Sco	SFA	16:10,−23:00	$ZYJHK$	cen. 75
Per-OB2	SFA	03:45,+32:17	$ZYJHK$	12.6
Hyades	OC	04:27,+15:52	K only	291
Coma-Ber	OC	12:25,+26:06	K only	78.5

Table 3. The GCS fields, with details of coverage in the 2-year plan. Types are open cluster (OC) or star formation association (SFA)

4.5 UDS 2-year plan

The UDS is a single 0.8 deg^2 Tile, centred on $(2^h18^m, -5°10')$, chosen to coincide with the Subaru/XMM-Newton Deep Survey field. This field lies just westward of the XMM-LSS field in the DXS. The 2-year plan is to cover the Tile to $K = 22.8$, i.e. full depth, and to $J = 23.8$, i.e. one magnitude short of full depth.

5 SURVEY OBSERVATIONAL IMPLEMENTATION

In this section we set out relevant details of the observational implementation that are needed for understanding the characteristics of the data. The observing procedures were adjusted in the interval between 05A and 05B, and relevant differences are detailed in the appropriate sections.

5.1 General details

Each survey is divided into 'projects'. Projects are a means of segregating observations for administrative purposes. In the shallow surveys, projects segregate observations by area, for example, the LAS is divided into several projects, the EDR containing data in the projects LAS1-4 (see Figure 2). In the deep surveys, projects simply provide a convenient way of dividing up observations between semesters.

Observations are packaged in 'minimum schedulable blocks' (MSBs). MSBs typically last one hour and are designed to be self contained in the sense that the sky frames for sky subtraction may be formed from the data itself. Each MSB has its own set of criteria for the conditions under which it may be executed. At the summit the UKIRT observing management program automatically schedules MSBs according to their observability (i.e. hour angle and airmass) and the current conditions (transparency, seeing, J-band sky brightness).

The basic unit of the surveys is the stack '*multiframe*' (see Section 10.1), which is the group of four images, one for each detector, formed by averaging the set of exposures made at the same base position within a given MSB. The region being surveyed is tessellated by these stack multiframes. The smallest contiguous region that can be surveyed is a Tile, requiring four base positions to fill in a solid angle of 0.77 deg^2.

Descriptions of the implementation of each survey employ the following observing terminology, defined by UKIRT, which we use with appropriate capitalisation to distinguish from the general term:

- *Exposure* - An Exposure is a single complete cycle of the detector readout mode, over a time specified as the Exposure Time, $t_{\exp}$ (referred to by the `expTime` attribute in the WSA).
- *Integration* - An Integration is a sequence of one or more Exposures, that are averaged by the data acquisition system, resulting in a single image being written to disk. An Integration is therefore the basic observational product. For all UKIDSS observations, Integrations comprise single Exposures.
- *Offset* - An Offset is an accurate shift in the telescope pointing between two Integrations. Integer-pixel Offsets are used for all UKIDSS Integrations, except in the case of Microstepping (see below). At UKIRT, Offsets smaller than $10''$ are fast, so all Offsets used in UKIDSS MSBs are smaller than this. Also, frames Offset by $< 10''$ may be combined without regard to WFCAM's variable pixel scale (see Section 6.3). Larger Offsets required rebinning of the data.
- *Microstep* - A Microstep is a special case of an Offset, where the step in X and Y has the size of either $n + 1/2$ or $n \pm 1/3$ pixels, n being an integer. These two cases are referred to as 2×2 and 3×3 Microstepping hereafter.

A variety of Offset patterns are used in the surveys, resulting in three different types of frame in the archive as follows:

- *Normal frames* - A Normal frame corresponds to an Integration.
- *Interleave frames* - A set of Microstepped frames (four or nine, for 2×2 or 3×3 Microstepping, respectively) are interleaved onto the sub-pixel grid, to form an Interleave frame (abbreviated 'Leav' elsewhere in this paper and in the WSA).
- *Stack or Interleave-Stack frames* - Where Microstepping has not been used, frames taken at different Offsets are registered, and averaged to form a 'Stack' frame. Where Microstepping has been used, the Interleave frames are registered and averaged to form an Interleave-Stack frame (abbreviated 'Leavstack' elsewhere in this paper and in the WSA).

Note that because the zero point for a frame relates counts per second to magnitudes, and because averaging is used at all points in combining frames, only $t_{\exp}$ is needed to calibrate any frame (rather than the total Integration time, t_{tot}).

5.2 Shallow surveys: LAS, GCS & GPS

The choice of $t_{\exp}$, whether to Microstep, and the number of Offsets, involves consideration of the relative importance of sampling, overheads, bad pixels and read-noise relative to sky noise. These reasons motivate the different implementation schemes detailed below. Between them, the three shallow surveys use three different implementation schemes, numbered 1 to 3 in Table 4. For each scheme, the table lists successively the scheme number, the filters to which the details apply, the Exposure time, the Microstepping (if used),

Scheme (Survey)	Filter	$t_{\rm exp}$ (s)	μ-step?	Offsets	$t_{\rm tot}$ (s)
1 (LAS, GCS)	ZY	20s	no	2-pt	40
	JHK	5s	2×2	2-pt	40
2 (LAS)	Y	20s	no	4-pt	80
	JHK	10s	2×2	2-pt	80
3 (GPS)	JH	5s	2×2	4-pt	80
	K	5s	2×2	2-pt	40
4 (DXS)	JK	5s	2×2	25-pt	500
5 (DXS)	JK	10s	2×2	16-pt	640
6 (UDS)	JK	10s	3×3	9-pt	810

Table 4. The different implementation schemes used for the shallow surveys, LAS, GCS & GPS

Category	Photometric	Seeing	J sky mag/arcsec^2
A	Y	$< 1.0''$	> 15.7
B	Y	$< 1.4''$	> 15.0
C	thin	$< 1.0''$	> 15.7

Table 5. The different categories of observing conditions allowed for LAS observations

the number of Offset positions (other than Microsteps) and the total Integration time $t_{\rm tot}$ making up the stacked frame.

5.2.1 LAS implementation

LAS observations are carried out in the filters Y, J, H, and K. The goal is to reach uniform depth in all fields. The MSBs comprise observations of a number of Tiles and are of two types, where the filters used are either the pair YJ or the pair HK. If an area has been covered by one pair, every effort is made to cover the same area with the other pair, within a month. Nevertheless, this is not a strict requirement. In order to make the most efficient use of the observing time, a wide range of conditions is used. The choice of MSB to execute depends on whether the conditions fall into one of the three categories listed in Table 5, defined by photometricity, seeing, and J-band sky brightness. Since these are the conditions pertaining at the start of the MSB, the actual conditions may be better or worse. The final criteria which define any data release are set at the QC stage (Section 8).

In 05A, observations were made in the four regions marked LAS1, LAS2, LAS3 and LAS4 in Figure 2. The combinations of filters, implementation strategy (Table 4), and conditions category (Table 5), used for each region are as follows: LAS1 and LAS4 ($YJHK$, 1, A), LAS2 ($YJHK$, 2, B), LAS3 (J, 2, C), which translates as follows: If conditions are photometric, with good seeing and dark sky, regions LAS1 and LAS4 are observed in all filters. If conditions are photometric, but either the seeing is poor or the sky is bright, or both, Integration times are doubled and LAS2 is observed in all filters. If there is thin cirrus but the seeing is good and the sky dark, Integration times are doubled and the first

epoch J-band observations in LAS3 are made. Because calibration is made using 2MASS stars in the frames themselves (Section 6.4), the extinction by cloud in these observations is corrected for. However, this correction accounts only for the average extinction over the frame, not spatial variation in extinction, hence the accuracy of the photometry will not be as good as under photometric conditions. This remains to be quantified.

5.2.2 GPS implementation

GPS observations are carried out in the filters J, H and K, using strategy 3 (Table 4). Depending on conditions, two different types of MSB are executed.

1) In photometric conditions, good seeing $< 0.8''$ at K and J sky brightness > 15.5 mag/arcsec^2, a single Tile is observed in filter order J, H then K, providing near-simultaneous observations of the same area.
2) In conditions of thin cirrus and good seeing $< 0.8''$ at K, first-epoch K-band observations of four Tiles are executed.

5.2.3 GCS implementation

GCS observations are carried out in the filters Z, Y, J, H and K using scheme 1 (Table 4), in seeing conditions $< 1.0''$. Depending on the transparency, two different types of MSB are executed.

1) In photometric conditions the full filter set is observed. For J sky brightness > 15.7 mag/arcsec^2, MSBs containing observations in ZYJ may be executed. There is no sky brightness constraint on MSBs containing observations in HK.
2) In conditions of thin cirrus first-epoch K-band observations are executed.

5.3 Deep surveys: DXS & UDS

The two deep surveys employ similar strategies. An MSB creates the necessary data to produce four stack multiframes covering a Tile in a single filter. Depth is built by repeating the MSB starting from a slightly different base position. For example, for the UDS, the centres are produced with a Gaussian distribution about the global field centre with a FWHM of $20''$, and truncated at a maximum offset of $2'$.

5.3.1 DXS implementation

DXS observations are carried out in the filters J and K. An MSB comprises observations in one of the filters, of a complete Tile. Implementation scheme 4 (Table 4) was used in 05A and implementation scheme 5 was used in 05B. The reason for the change to longer Integration times was to reduce overheads. For the EDR, DXS observations required seeing $< 1.1''$ and transparency conditions of thin cirrus or better.

5.3.2　UDS implementation

UDS observations are carried out in the filters J and K. An MSB comprises observations in one of the filters, of the complete UDS Tile. Implementation scheme 6 (Table 4) was used. For the EDR the required observing conditions for J were seeing $< 0.85''$, sky brightness > 16.0 mag/arcsec^2, and for K, seeing $< 0.75''$ with no sky brightness limit. Required transparency was thin cirrus or better, for all observations.

6　PIPELINE AND CALIBRATION

Pipeline processing and archiving for all WFCAM data, including the UKIDSS surveys, is provided by the VISTA Data Flow System Project (VDFS), which is a collaboration between Queen Mary University of London, Cambridge, and Edinburgh. The UKIDSS consortium interacts closely with the VDFS team and has primary responsibility for the final QC stage in producing the UKIDSS products.

At the summit there is a data stream for each detector. Thus, every Integration results in a single FITS file being written to each of four LTO tapes. After transfer to CASU[2] but prior to pipeline ingest, the four FITS files of an Integration are combined into a single multi-extension FITS (MEF) file. A MEF file has one header per extension and a primary header that contains general observation information together with the data acquisition protocols used, which trigger the appropriate pipeline processing components. These are described in this section.

The output of the pipeline is a set of reduced uncalibrated Normal frames and photometrically and astrometrically calibrated Stack/Leavstack frames, as well as catalogues of images detected in the Stack/Leavstack frames. Merging of catalogues across bands is undertaken in the archive. We refer the reader to Irwin et al. (2006) for further information on all details contained in this section.

6.1　Pixel data processing

The pipeline processes data on a night-by-night basis. The data files fall into one of three categories; science frames (including calibration standards), (dawn) twilight flatfields, and darks. The first pipeline step creates a set of master darks by stacking frames segregated by Exposure time and read mode. The appropriate master dark is then subtracted from all frames. Aside from hot pixels, the dark current is very low for the WFCAM detectors and the main effect of dark subtraction is to remove the majority of the reset anomaly[3].

The data are then flattened by the appropriate master twilight flat, for the particular filter. Master twilight flats are updated at least monthly. These are used in preference to dark–sky flats which can be corrupted by thermal emission

and fringing (although the latter is at a very low level in the WFCAM detectors). We note in passing that detectors 1 and 4 are respectively the most and least sensitive, with a quantum efficiency ratio of ~ 1.3 in Z, falling to ~ 1.2 in K. This variation is accounted for by normalising each detector's flatfield by the median of the counts in all four detectors.

The next stage is to subtract the bias curtaining, described in Section 3. The curtaining pattern is mirrored, rotated, in each quadrant. Therefore, the varying bias level may be established by appropriate filtering of the data in 4×1024 pixels. Following this, a running median–filtered sky–correction frame is created and subtracted for removal of residuals, including images due to dirt and marks on the field lens, either from scattered light or thermal emission. The term 'sky correction' means subtraction of residuals relative to flat sky, i.e. the average sky count is preserved.

Different versions of the pipeline were used to process 05A (LAS, GPS, GCS, some DXS) and 05B (UDS, some DXS) data. The 05B version has improved sky correction and a module to correct cross-talk images. Presently, the pipeline makes no correction for persistence. This is currently being characterised and a later version may include removal of the effect.

If appropriate, the frames are then interleaved (Section 5.1). The final stage is the creation of a Stack or Leavstack frame by weighted averaging. Each frame is weighted by the product of the inverse of its noise variance and the confidence map. The confidence map is derived principally from the master flatfield and is normalised to have a median of unity, but additionally dead pixels, pixels with poor sensitivity and pixels with unpredictable levels (e.g. some hot pixels) are given zero confidence. For the DXS and UDS, where multiple visits are made, the Leavstack frames are themselves stacked, but at a later stage (see Section 9).

6.2　Catalogues

A source extraction routine based on the methodology of Irwin (1985) is run on the stacked images. Sources are identified with groups of four or more connected pixels that all lie more than 1.5σ above the local background sky level (1.25σ for frames interleaved to $0.2''$/pixel or $0.133''$/pixel). A global background following algorithm (Irwin & Trimble 1984) is used to track the varying sky level over each frame, on a scale of $25.6''$ (i.e. 64, 128 or 192 pixels for no, 2×2 or 3×3 Microstepping). This scale represents a compromise between being small enough to follow rapidly varying background and large enough to sample sufficient sky pixels outside objects. The initial background value in each $25.6'' \times 25.6''$ block is computed using an iterative k-sigma clipped median estimator, after removing bad pixels. The resulting array of block values is then filtered to remove outliers due, for example, to bright stars. The filtered coarse grid is then bi-linearly interpolated back to the original pixel grid.

A set of parameters is measured for each detected object. These are listed in Table A1. Fluxes are corrected for the flatfield error, caused by the variable pixel scale across the field of view (Section 6.3). Errors are computed from photon count, read-noise and local background error. A number of parameters that will be included in later versions

---

[2] The web page *http://www.ast.cam.ac.uk/~wfcam* provides access to the WFCAM raw data and includes summaries of the progress of the observing and data reduction for the surveys.
[3] This is an additive component varying in amplitude in a ramp–like manner across a frame, as a consequence of the decaying capacitative behaviour of the detector, and the time delay between the reset and the first read, as a function of position.

of the pipeline, including PSF magnitudes and Sersic-profile fits are also listed. In addition, a variety of quality control parameters are recorded for each stacked detector frame, including average stellar ellipticity and seeing, as well as the sky brightness and the photometric zero point. In deriving object parameters, the current version of the pipeline does not make use of the weight information in the confidence map. The measured parameters include a series of 13 circular-aperture fluxes of fixed aperture size, listed as `aperFlux[1-13]`. Apertures are 'soft-edged' in the sense that flux in pixels bisected by the aperture boundary is scaled according to the fraction of the pixel enclosed. All aperture fluxes (and the corresponding magnitudes `aperMag[1-13]`) in this set have the aperture correction applied, as determined from bright stars in the field. This means that for point sources, these aperture magnitudes approximate total magnitudes so that for typical seeing, the parameter `aperMag3` provides the most accurate estimate of the total magnitude. There are three further aperture fluxes, the Petrosian, Kron and Hall fluxes, where the aperture size is defined from measurement of the surface–brightness profile. These three fluxes are not corrected for flux outside the aperture. Merged objects are deblended in a manner which avoids double counting of flux.

6.3 Astrometric calibration

Astrometric calibration incorporates a cubic radial distortion term, i.e. where the relation between $r_{\rm true}$, the true on-sky angular distance from the optical axis, and r, the distance measured in a WFCAM image, takes the form

$$r_{\rm true} = r + kr^3 \,. \tag{1}$$

The constant k has a small wavelength dependence. Measured values at H and K are $-50/{\rm radian}^2$ and $-53/{\rm radian}^2$, respectively, for r in radians. Higher order distortion terms are insignificant, compared to the specified absolute systematic accuracy of $< 0.1''$ RMS. Calibration is achieved by a fit to the coordinates of objects in the 2MASS point source catalogue, solving for distortion parameterised by k, and a six-parameter linear transformation;

$$x' = {\rm a}x + {\rm b}y + {\rm c} \quad ; \quad y' = {\rm d}x + {\rm e}y + {\rm d} \,, \tag{2}$$

which allows for translation, scaling, rotation and shear. Since 2MASS astrometry is based on Tycho 2 and is in the International Celestial Reference System (ICRS), so too is WFCAM astrometry. This does not require an Equinox to be specified and for most practical purposes this is (almost) equivalent to Equinox 2000 in FK5[4]. Once computed, the astrometric solution is written into the catalogue MEF files and back-propagated to the stacked and component image MEF files.

6.4 Photometric calibration

The procedures for photometric calibration of UKIDSS data are still being refined. The specified absolute systematic ac-

---

[4] MEF files have the FITS keyword RADECSYS = 'ICRS' set. For backwards compatibility with existing software, EQUINOX = 2000.0 is left as is.

curacy is 0.02 mag in each band. Initially it was expected that calibration would be achieved through setting up fields of WFCAM standards, which themselves would be calibrated to UKIRT Faint Standards. Instead the EDR data have been calibrated using 2MASS stars in the frames themselves, applying colour equations to convert 2MASS photometry to the WFCAM system (see Hewett et al. 2006, for details of the WFCAM filters). Further improvements of this method are anticipated, and it now appears likely that the specified accuracy can be achieved through this route. In this section we describe the photometric calibration of the EDR, which summarises the current status of our programme to use 2MASS stars to calibrate UKIDSS fields.

The motivation for basing the calibration on 2MASS includes:

• The 2MASS global calibration is accurate to better than 2% across the entire sky (Nikolaev et al. 2000).
• In each WFCAM field there is always an abundance of unsaturated stars, with 2MASS errors < 0.1 mag (typically 60-1000, depending on galactic latitude).
• Measuring the calibrators at exactly the same time as the targets enables photometric calibration even during non-photometric conditions (accuracy limited by the uniformity of the cloud cover).

To calibrate the frames, the first step is to identify unsaturated WFCAM sources that appear in the 2MASS Point Source Catalogue, with 2MASS errors < 0.1 mag. The 2MASS photometry is transformed into the WFCAM $ZYJHK$ system using the following empirically–derived colour equations:

$$
\begin{aligned}
Z_{\rm WFCAM} &= J_{\rm 2MASS} + 0.95(J_{\rm 2MASS} - H_{\rm 2MASS}) \\
Y_{\rm WFCAM} &= J_{\rm 2MASS} + 0.50(J_{\rm 2MASS} - H_{\rm 2MASS}) \\
J_{\rm WFCAM} &= J_{\rm 2MASS} - 0.075(J_{\rm 2MASS} - H_{\rm 2MASS}) \\
H_{\rm WFCAM} &= H_{\rm 2MASS} + 0.04(J_{\rm 2MASS} - H_{\rm 2MASS}) - 0.04 \\
K_{\rm WFCAM} &= K_{\rm 2MASS} - 0.015(J_{\rm 2MASS} - K_{\rm 2MASS})
\end{aligned}
$$

A zero point is then computed for each star, as

$$ZP_i = m_i + 2.5 \log_{10}(N_i/t_{\rm exp}) \tag{3}$$

where N_i is the parameter `aperFlux3` for the star, i.e. the total counts in ADU of source i, estimated by aperture correction of the summed counts in an aperture of radius $1''$ and additionally corrected for extinction, using a default extinction of 0.05 mag per unit airmass (assumed for all nights and all filters). The photometric zeropoint for a given stacked detector frame is then simply the median zeropoint over all unsaturated stars. The extinction correction would not be needed simply for calibrating the data, but allows the zero points to be inter-compared, to provide a measure of photometricity. Note that since counts in interleaved frame pixels are the counts in the full WFCAM pixels from the progenitor Normal frames, when comparing zero points between different frames, a correction of $2.5 \log_{10}(4)$ or $2.5 \log_{10}(9)$ must be subtracted from the zero points of frames Microstepped by 2×2 or 3×3 respectively.

The accuracy of the astrometry and photometry in the EDR data is quantified in Section 8.

7 DATA ARTIFACTS

There are a variety of artifacts in the images which compromise the quality of the data in a number of ways. In particular, they give rise to false detections, with the consequence that a small fraction of the entries in the catalogues are for objects that have apparently interesting colours, but are not real. For reference purposes we catalogue the various artifacts here, as a prelude to the next section, where the QC procedures are described. Figure 3 provides a montage illustrating the various effects.

Persistence images

Persistence images of a saturated star can appear over several subsequent frames and are not currently treated in the pipeline. The brightness of the persistence image is a function of source count rate, wavelength (i.e. filter), and number of reset/reads. Persistence images are characteristically the size of the saturated part of their progenitor image. Images persisting across a number of frames will follow any Offset pattern employed and in such cases the effect usually stacks out.

The flare image marked 'F' in Figure 3 is also a result of persistence and is often visible in 05A data in the first frame taken after a filter change (because the detector has been exposed to unfiltered light and consequently saturated; see Section 3). For the 05B data, a short sequence of dark frames following each filter change was implemented, to flush persistence images. In these data, the flare image is thus largely removed.

Cross-talk images

The zoom image in Figure 3 of a portion of detector 3 illustrates the problem of cross-talk. Here, a sequence of spurious images can be seen, which are caused by the bright star. In general, cross-talk images appear in some or all of the 7 other channels of the quadrant in which the star is located. The images are always offset across the channel width by an integer multiple of 128 pixels (256 or 384 pixels for 2×2 or 3×3 Microstepping, respectively). The appearance of the cross-talk images depends on the counts in the star, and, for bright stars, the shape matches the spatial derivative of the profile of the star. Therefore, for bright unsaturated stars the cross-talk images have a half-moon appearance, while for saturated stars, where the counts at the centre of the image are constant at the saturation value, the cross-talk images have the curious washer appearance shown. Cross-talk images in the channels adjacent to the star have features at the level of $\sim 1\%$ of the flux difference between adjacent pixels in the star, dropping to lower levels further from the source.

Cross-talk images are particularly pernicious because they appear in the same location relative to the bright star, for all filters. Therefore the detections are matched across bands and the objects appear in the catalogues as entries with peculiar colours.

Channel bias offsets

In a few percent of frames the counts in any channel may be offset high or low by a few counts, or more rarely by tens of counts. Because of the lower sky counts, the effect is more often visible in the shorter wavelength bands Z, Y and J. Two channels in detector 4, marked 'C' in the figure, are particularly prone to this variable bias level. The offset can vary from one frame to the next and therefore is not effectively removed by subtraction of a dark frame. Very occasionally all the channels in a detector are afflicted, such that the entire channel pattern is visible, as in the case of detector 4 in the illustration.

Channel bias offsets are particularly troublesome in interleaved data, since every fourth pixel (or ninth in 3×3 Microstepping) is offset in level, resulting in a 'bed-of-nails' pattern. In the worst cases, the bias offsets confuse the object detection algorithm, resulting in a large number of spurious sources in the channel. We have attempted to identify the worst cases and removed the frame and catalogues from the release database. Both hardware and software solutions to the problem of channel bias offsets are being pursued.

Bright moon ghosts

In some circumstances, apparently when the moon is shining directly onto the field lens, bright ghost images occur, such as the image marked 'G' in detector 4 in Figure 3. The appearance of the ghosts depends on the angle of inclination of the moon relative to the optical axis. The most common case, of the type illustrated, occurs when the moon is less than $30°$ from the target. At larger angles, highly elongated arcs sometimes appear. The exact cause of these images is under investigation. It is possible that the ghosts arise from reflection off the mounting arrangement of the autoguider auxiliary lens at the centre of the field lens.

We have attempted to identify all the brightest examples of moon ghosts, and remove the affected frames and accompanying image catalogues. Moon ghosts occur both in 05A and 05B data, affecting nearly 3% of the fields observed. For future WFCAM campaigns, fields within $30°$ of the moon will be avoided. Additionally a baffle extending above the field lens will be installed, which will further reduce the problem.

Images of marks or dirt on the field lens

Because the field lens (Section 3) is located close to an intermediate focus, marks or dirt on the lens, are visible in some frames. The three worst examples are marked 'L'/'L*' in Figure 3. The two large blotches, marked 'L*', correspond to the locations of support pads used in the installation of the lens. These are particularly visible in scattered light when the moon shines directly on the field lens (the case shown is a particularly bright example). Their visibility has been much reduced since the underside of the lens was cleaned between semesters 05A and 05B. There are also numerous smaller elliptical-ring images, that are caused primarily by dust on the upper surface of the lens. These images are visible both in scattered light and in thermal radiation. They are more prevalent in the earliest data, until more frequent cleaning of the upper surface was introduced. As a rule, when illumination from the moon is fairly constant, these spurious images are successfully removed by the pipeline, at the stage of sky correction. However, the problem is more difficult to treat if the intensity is variable, for example as the moon transits into or out of the dome slit. Avoiding observations close to the moon, and installation of the field-lens baffle, should both act to reduce the problem of images of marks or dirt on the field lens.
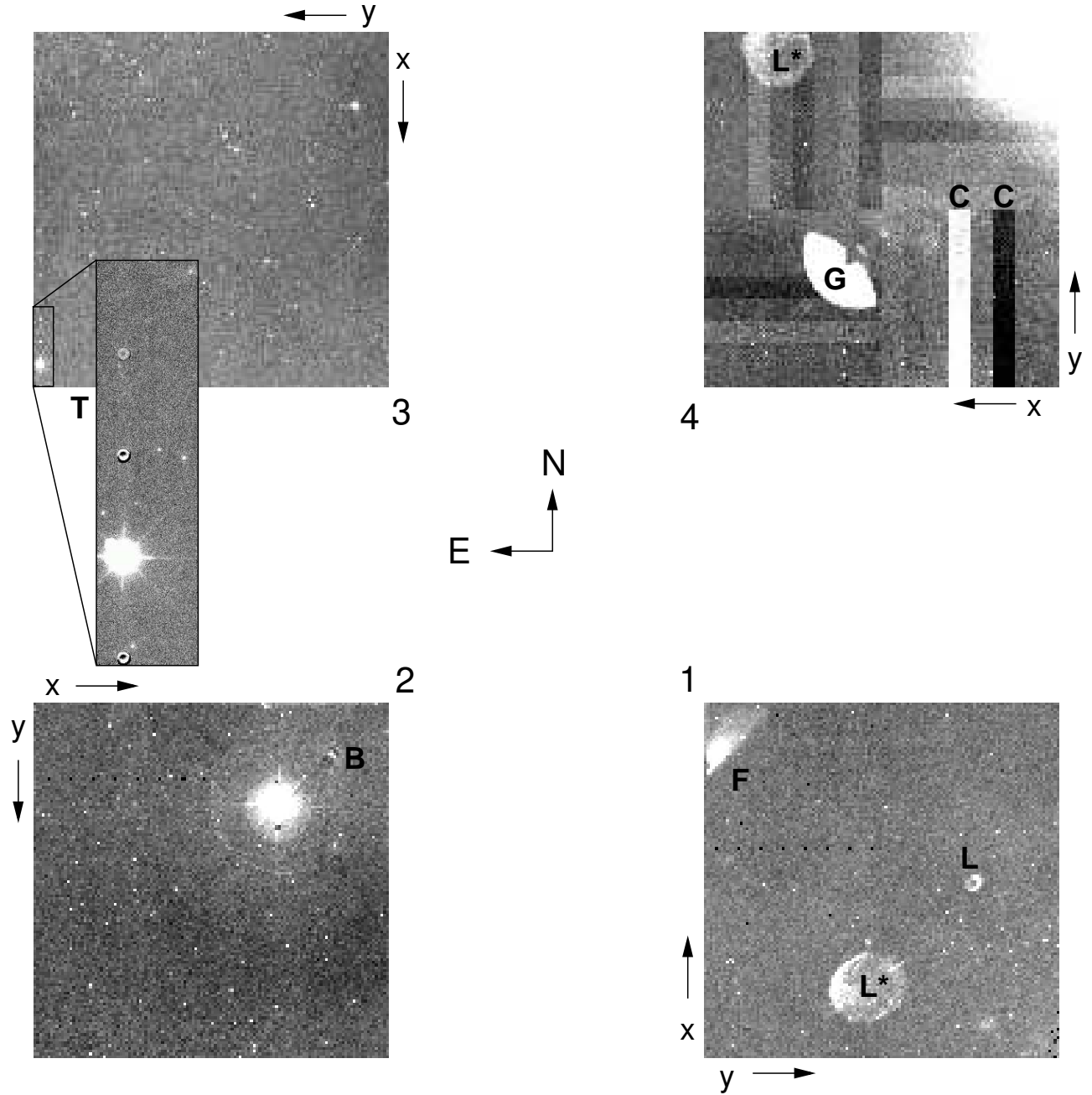
Figure 3. WFCAM focal plane showing composite of various data artifacts that can arise in WFCAM data, described in detail in the text. As marked, North is up and East to the left. Data artifacts key: F - flare persistence image that appears after filter changes, T - cross-talk image sequence associated with bright star, C - the two worst channels with variable bias level, G - bright ghost from moonlight shining on the field lens, L - images caused by marks or dust on the field lens (L* are marks left by the lens handling jig), B - 'bow-tie' feature in the halos of bright stars.

Diffraction pattern for bright stars

The image of a bright star in detector 2 is shown in Figure 3. The diffraction pattern shows 8 spikes, from two spiders, one supporting the secondary, and the other the guider auxiliary lens, above the field lens. The spikes can extend to large angles, $\sim 20'$, and therefore may be visible in some frames where the bright star itself is not visible. There is a low-level feature in the point spread function, marked 'B' in Figure 3, which has the shape of two bow-

ties. Similarly this feature can be visible in some frames, where the star itself is outside the field of view.

8   UKIDSS DATA QUALITY CONTROL

This section is divided into two. The first part describes the UKIDSS QC procedures and summarises the fraction of data rejected. The second part quantifies the accuracy of the

astrometric and photometric calibration. The areal coverage and depth of each survey are provided in the next section.

8.1 QC procedures and data quality

The output of the pipeline is a set of Normal, Leav and Stack/Leavstack frames and catalogues of detections in the Stack/Leavstack frames. These data are ingested by the archive, where a process of curation results in seamless catalogues of objects matched across bands. In collaboration with WFAU we are developing a set of QC procedures, specifically for UKIDSS data, that are applied at various points in the ingest and curation processes. The aim of the QC is to eliminate data that are either corrupt (i.e. where something went wrong in the data-train and the data are meaningless), or bad (i.e. where the data are unusable, because of a bright moon ghost, for example), and then to apply a set of cuts that define 'survey quality' using a number of measured parameters, such as seeing and depth. The definitions for each survey of 'survey quality' are still being refined, with the aim of finalising a set of rules that will be applied rigidly to DR1. We have used the EDR to develop the rules. For the EDR we have defined the cuts (see below) by inspecting the distributions of the relevant parameters and clipping the tails. Bearing in mind the poorer image quality of the 05A data, we anticipate that the rules applied to DR1 will be more stringent than those applied to the EDR.

First, a set of book-keeping checks are made to identify corrupt data resulting from glitches in the data-train. For example, if the wrong information is written to the headers, a set of files may have been processed with the wrong algorithm. For a particular field, observed with a particular filter, the checks include verifying that the correct complement of files and catalogues exist, that data are present for each detector, and that the header parameters are meaningful. Depending on the nature of the problem, the entire complement of files and catalogues is eliminated either for a detector, or for the full set of four detectors.

Three checks are made to identify bad data. Every stack frame is inspected visually for cases of bright moon ghosts, trailing (i.e. where guiding was lost), poor sky correction, or particularly bad cases of channel bias offsets. A second check for cases of poor sky correction is made using the attribute `skySubScale`. This is the scaling of the correction frame made in the sky-correction step. A check is made of all normal frames, for cases where the parameter is unusually high or low. A third check for bad data is made by identifying frames with large numbers of false objects, where the detection algorithm has been confused. This can arise in cases of large channel bias offsets and also sometimes where the sky correction is poor. The check is made by searching the merged catalogues for frames containing unusually large numbers of objects detected in one band only.

The cataloguing procedure results in a set of parameters that are useful for characterising the quality of the data, for each detector of a stack multiframe. Listing the parameters by the name stored in the WSA table `Multiframedetector` (Section 10), these are: `seeing` (the average image FWHM of detected stellar sources), `avStellarEll` (the average ellipticity of detected stellar sources), `skyLevel` (the average counts per pixel in blank sky), `skyNoise` (σ_{sky}, a robust measure of

the standard deviation of counts in the sky), and `PhotZPCat` (m_0, the photometric zero point). From these, we compute the 5σ detection limit for a point source m_d, as 5 times the standard deviation of the counts in an aperture, corrected for flux outside the aperture, by the aperture correction m_{ap}

$$m_d = m_0 - 2.5\log_{10}(5\sigma_{sky}(1.2N)^{1/2}/t_{exp}) - m_{ap} \qquad (4)$$

where N is the number of pixels in the aperture, and the factor 1.2 accounts for the covariance between pixels.

The interplay between these various parameters is illustrated in Figure 4, which plots depth m_d against ellipticity, seeing, sky brightness and zero point, for the LAS data in the EDR database, i.e. all LAS fields with data in all four filters which pass the QC cuts (defined below). A number of points are worth noting. The plots show the expected anti-correlations between depth and seeing, and depth and sky brightness (most clearly seen in the H-band plot). The effect of thin cloud is also noticeable, e.g. in the K band, in the correlation between depth and zero point. In most cases, the average ellipticity is < 0.1 with a tail to larger values. Large ellipticities may arise in fields where the guide star is very faint and guiding was lost. This occurred occasionally in the LAS, where, of all the surveys, the surface density of suitable bright guide stars is lowest. We have since adjusted our tiling strategy to minimise this problem.

For the EDR, we applied seeing limits for each survey, marginally greater than the limits specified for the observations, as follows; DXS ($1.25''$), LAS ($1.2''$), GCS ($1.2''$), GPS ($1.0''$) & UDS (J $0.9''$, K $0.8''$). These were applied to the average measured value for the four detectors of each stack multiframe, i.e. the whole multiframe was accepted or rejected on this measure. A cut on ellipticity < 0.25 was applied to all data. For most fields a cut was made on zero point at a level of 0.2 mag extinction from the modal (i.e. photometric) value. In other words, a number of fields have been calibrated through thin cloud. This figure of 0.2 mag is under review, pending an analysis of the uniformity of photometric calibration under such conditions. For the DXS and UDS fields and the first-epoch single-band observations in the shallow surveys, extinction up to 0.3 mag was permitted, although conditions this bad are rare in the data. Finally, to ensure uniformity, a cut on depth was made at 0.4 mag brighter than the modal value for each filter in each survey.

Discounting corrupt data removed by the book-keeping stage of QC, the quantity of sub-standard data rejected by the QC procedure over the whole of the EDR (i.e. the EDR+ database) as a fraction of each survey is as follows: LAS 23.0%, GPS 27.3%, GCS 25.9%, DXS 19.6% & UDS 0.0%. The corrupted data approximately account for an extra third of these fractions per survey. Of the corrupted data, $> 95\%$ will be recovered by re-processing in a later release.

The proportion of data rejected, nearly 25% overall, is rather large, but this figure should fall to below 10% in the future. Of the 25%, about 10% represents repeat observations, because the first observations were unsatisfactory. Revised procedures for identifying deteriorating conditions and interrupting the observations will reduce this figure. A further substantial fraction, about 7%, can be attributed to scattered light or bright ghosts (and associated sky gradients), when observing near the moon. These issues will be dealt with in more detail in the paper accompanying the
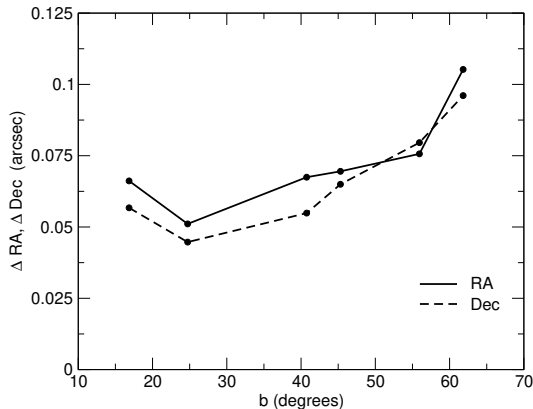
Figure 5. Astrometric consistency of duplicate objects found in overlapping detector frame edges in the LAS and GCS. Plotted is the RMS/$\sqrt{2}$ of the distribution of the median difference in RA or Dec of duplicate stellar-like objects (with $12 \leqslant J \leqslant 18$) per detector overlap area.

First Data Release, but have now (July 2006) been solved. A further 3% of frames are rejected for a variety of reasons, and the final 5% are frames which are outside the quality control cuts, for seeing, cloud etc., where seeing accounts for the majority. The implementation strategy allows for observations under a very wide range of conditions (seeing, sky brightness, cirrus) in order to make the most efficient use of the observing time available. Consequently the figure of 5% of frames observed in poor conditions is viewed as acceptable.

8.2   Calibration accuracy

The results of internal and external checks of the accuracy of the astrometric and photometric calibration are summarised here.

8.2.1   *Astrometric calibration*

Internal astrometric accuracy

The astrometric calibration, using 2MASS (Section 6), will be accurate to the extent that the functional form of the transformation applied is an accurate representation of the mapping between WFCAM pixel coordinates and equatorial coordinates, and there are sufficient 2MASS stars in the field. An internal check of the astrometric accuracy is possible by considering the consistency of the measured positions of objects observed twice, because they lie in overlapping edges of detector frames in adjacent fields. This will be a stringent test, since any systematic errors are likely to be largest at the frame edges. Figure 5 shows the result of this analysis for the J band, for the LAS and GCS. For each overlap region, the median value of the difference in RA and in Dec was computed for all stellar-like objects detected twice. The RMS (divided by $\sqrt{2}$ to give the systematic error on a single measurement) of this median difference, for all the overlap regions, is plotted against galactic latitude. At b$\sim 20°$, the error in RA and Dec is $\sim$ 50mas in each coordinate, rising to $\sim$ 100mas at b$\sim 60°$, where the fields contain fewer 2MASS stars for computing the solution.

External astrometric accuracy

If we assume that any systematic errors in the 2MASS astrometry itself will average out over many fields, we can measure the systematic errors in the astrometry around the WFCAM focal plane, by computing the differences between calibrated WFCAM positions and 2MASS positions, and averaging over observations of many fields at the same position on the detector. The result for $\sim$1100 fields, representing a week of EDR JHK observations, is shown in Figure 6. The plot shows the average residuals for all stars detected at S/N> 10. The size of the averaged RA and Dec residuals is 23mas RMS on each coordinate. With the current calibration scheme, this represents the limiting accuracy achievable, for the case of a field containing many 2MASS stars. The scatter for individual stars contributing to the plot is 80mas in each coordinate, which represents the random errors on the 2MASS coordinates. This gives an indication of the accuracy achievable in a field containing few 2MASS stars. Subject to further analysis, to confirm that the systematics plotted in the figure are stable, they will be corrected for in future releases.

8.2.2   *Photometric calibration*

Internal photometric accuracy

A similar check using the overlap regions has been made to estimate the internal photometric accuracy. The results are shown for the J band in Figure 7. As before, the median offset in photometry of stellar-like objects is computed for each overlap region and the RMS/$\sqrt{2}$ computed for all overlap regions. The results are plotted as a function of galactic latitude. In this case there is no visible trend with galactic latitude, and the average error is slightly less than 0.04 mag. Because the measurements are made at the edges of each detector, this probably overestimates the internal error representative of the whole field.

External photometric accuracy

Because of the large number of 2MASS stars in each field (Section 6.2), the accuracy of the photometry will be set by systematic errors in the 2MASS photometry and the accuracy of the colour transformations. For the 05A and 05B semesters, hourly observations were made of fields containing UKIRT faint standards (Hawarden et al. 2001), in all the broadband filters. These observations have been calibrated using 2MASS in exactly the same way as our UKIDSS fields. Therefore comparison of the 2MASS-calibrated photometry of the UKIRT faint standards, against the published values provides an external check of the accuracy.

The results for 600 measurements of 46 standard stars, measured on 19 photometric nights, for J, H and K are plotted in Figure 8. We find that the RMS scatter for these measurements is less than 2%, which is the UKIDSS requirement for photometric accuracy (see Hodgkin et al. 2006).

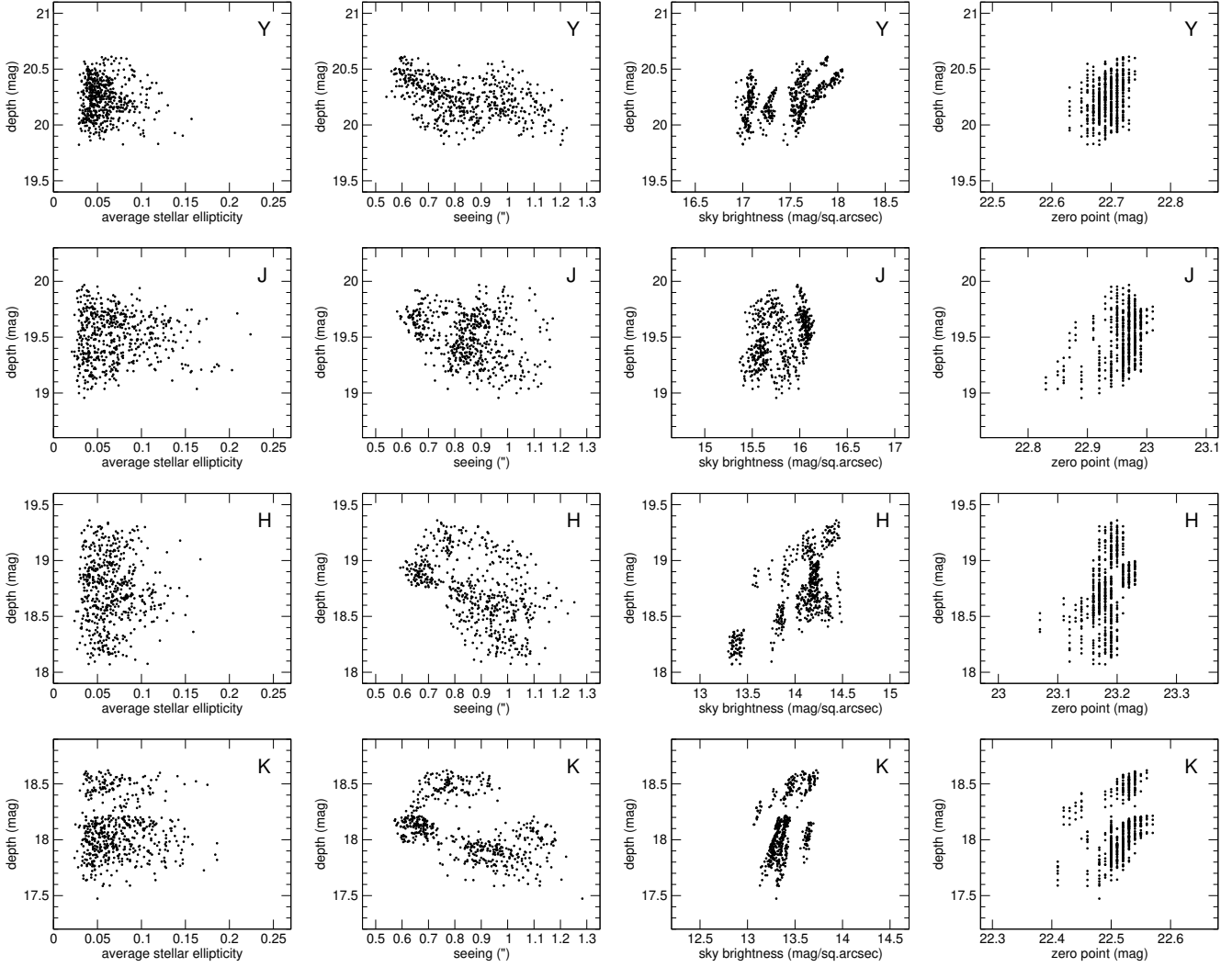The quality of the Z and Y calibration has not yet been quantified.

Figure 4. LAS data quality, plotting depth from equation (4) versus average stellar ellipticity, seeing, sky brightness and zero point in Y, J, H & K. Each point represents one detector frame in the EDR database. Note that a few points lie beyond the seeing limit of $1.2''$ since the cut was applied to the average multiframe seeing, not individual detector frames.

9   THE CONTENTS OF THE EDR

This section provides an overview of the contents of the EDR, including maps of the areas covered and details of the depths reached. The three shallow surveys LAS, GPS & GCS are described first, followed by the two deep surveys, DXS & UDS.

9.1   Shallow survey data

LAS, GPS and GCS data in the EDR were observed exclusively in semester 05A, between the dates 15th May 2005 and 20th June 2005. Table 6 provides details of the area covered by each survey. The first column lists the survey, and the second column provides the area covered in the EDR database, i.e. fields with observations in all filters for that survey. The next five columns list the area covered in the EDR+ database, by filter. The final column provides the summed area of fields covered by any filter. Note the large coverage in J in the LAS and in K in the GPS, because

Survey	EDR DB	Z	Y	EDR+ DB J	H	K	any
LAS	27.3	-	33.5	89.4	57.3	51.0	114.2
GPS	14.9	-	-	16.8	17.8	57.9	59.7
GCS	7.0	13.4	14.4	16.0	32.1	29.7	38.3
sum	49.2	13.4	47.9	122.2	107.2	138.6	212.2

Table 6. Coverage of the shallow surveys ($\deg^2$) in the EDR and EDR+ databases.

of the inclusion of first-epoch observations in the particular filter.

The depths reached in the three shallow surveys are summarised, by filter, in Table 7. The quantity listed is the 5σ depth for a point source, computed using equation 4. Two columns are provided for each survey. The first column lists the median value of the depth measured for all detector fields in the EDR database. The second column lists the same quantity, but restricted to fields in which the seeing was <
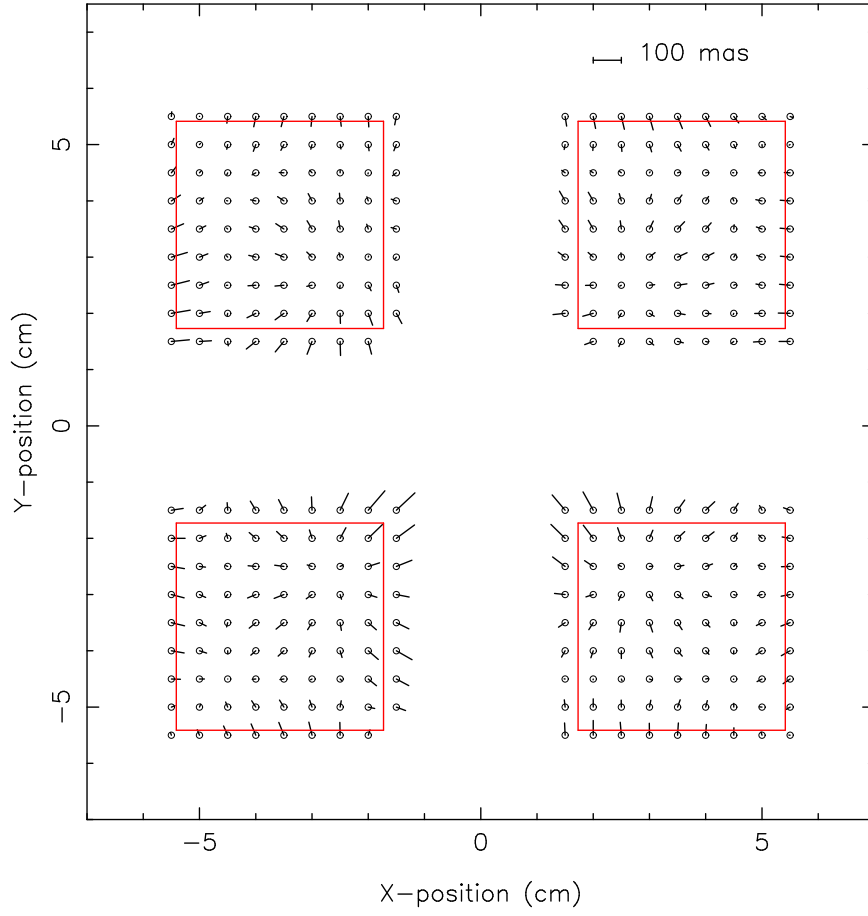
Figure 6. Distribution of astrometric systematic errors across WFCAM's field of view, calculated by averaging the residuals from 2MASS of WFCAM observations of ∼150,000 stars per detector.

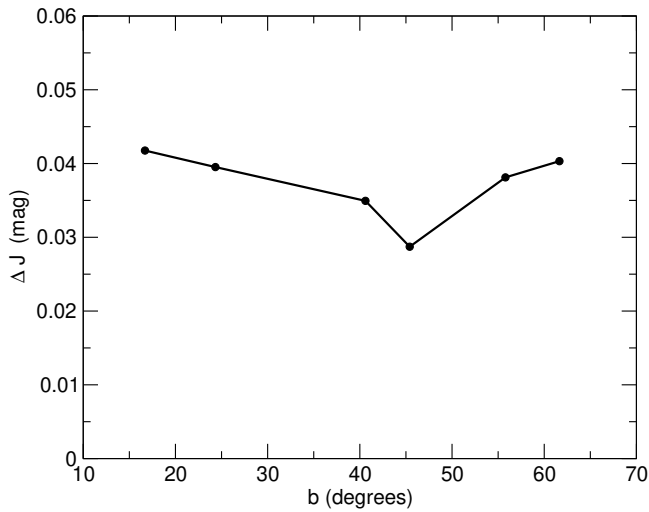**Figure 7.** Photometric consistency of duplicate objects found in overlapping detector frame edges in the LAS and GCS. Plotted is the RMS/$\sqrt{2}$ of the distribution of the median difference in J band magnitude of duplicate stellar-like objects (with $12 \leqslant J \leqslant 18$) per detector overlap area.
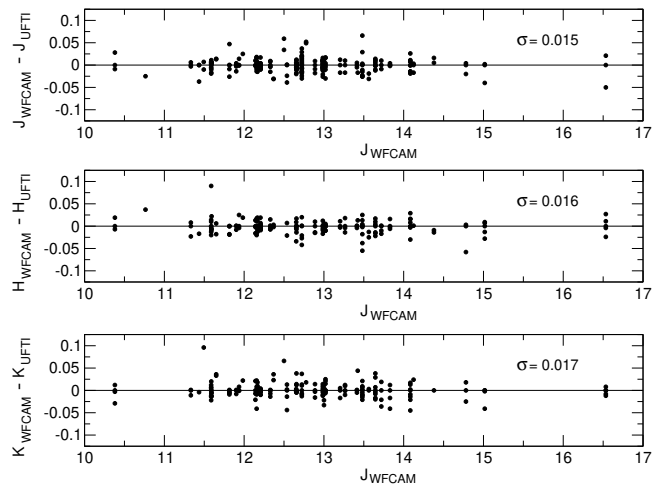

Figure 8. Difference between 2MASS calibrated WFCAM magnitudes and UFTI magnitudes of 46 UKIRT faint standard stars in J, H & K as a function of WFCAM J magnitude.

$1''$. Because the image quality improved between semesters 05A and 05B, we expect that most of the data in future releases will have seeing $< 1''$, so quantities in the second

Filter	LAS all	LAS $< 1''$	GPS all	GPS $< 1''$	GCS all	GCS $< 1''$
Z	–	–	–	–	20.29	20.40
Y	20.23	20.25	–	–	19.92	20.05
J	19.52	19.51	19.51	19.51	19.40	19.46
H	18.73	18.79	18.67	18.67	18.79	18.80
K	18.06	18.12	17.74	17.74	18.12	18.12

Table 7. The median 5σ point source depth by filter, in the EDR database, for the three shallow surveys, LAS, GPS & GCS. The two columns for each survey are for all seeing and just those data with seeing $< 1''$.

column are expected to be more representative of 'survey quality'. Nevertheless the differences are quite small.

The values quoted for the GPS deserve comment. The total integration times for the J and H bands are 80s, twice as long as for the LAS and GCS in these bands, while the total integration time in the K band, 40s, is the same as for the LAS and GCS (see Table 4). Taking the integration times into account, the GPS data are less sensitive than the LAS and GCS data by 0.4 mag on average, over the JHK bands. These values are for the EDR database and therefore are for fields within $1°$ of the plane. The lower sensitivity is attributed to unresolved stars in the background increasing the sky noise. Because nearly all the data have seeing $< 1''$, the depths quoted in the two columns are identical for the GPS.

Figures 9 to 12 provide maps of the sky coverage for the three surveys. In each map, every detector is shown. Dark grey tiles mark EDR database fields and light grey tiles mark the additional fields in the EDR+ database. For the purposes of comparison, all the coverage plots for the shallow surveys have the same scale. We now briefly describe the maps for each survey.

In the LAS, data were taken in the projects LAS1 − 4, shown in Figure 2. Maps of the areas covered are provided in Figures 9 and 10. All four projects provide data to the EDR+ database, but data in the EDR database is confined to projects LAS2 and LAS4. The majority of the data in the EDR database is in LAS4, which covers the eastern half of the Millennium Galaxy Catalogue (MGC) strip (Liske et al. 2003). The project LAS3 contains exclusively first-epoch data in the J band.

GPS data in the EDR+ database are limited to the range of galactic longitude $-2° < l < 107°$. The coverage map is provided in Figure 11. Within this region, the EDR database coverage is specifically limited to $|b| < 1°$, $-2° < l < 107°$ and $|b| < 5°$, $30° < l < 45°$. Care should be taken in interpreting the GPS catalogues in regions of nebulosity, which can cause difficulties for the background-following algorithm.

Finally, for the GCS, the EDR+ database holds data for the Sco. star forming association and a small region in the Coma-Ber open cluster. Coverage in the EDR database is confined to the Sco. star forming association. The coverage map is provided in Figure 12.

9.2 Deep survey data

DXS data span semesters 05A and 05B between the dates 9th April 2005 and 27th September 2005. Data were taken in all four DXS fields. UDS data are from semester 05B only, from the 12th to the 27th September 2005.

The basic unit of the deep surveys is the Leavstack frame that results from the implementation schemes detailed in Table 4. For the DXS the frames are interleaved at the scale $0.2''$/pix, and are the result of total integration times of either 500s (05A) or 640s (05B). For the UDS, the frames are interleaved at the scale $0.133''$/pix and are the result of a total integration time of 810s. Leavstack frames are created by interleaving on a sub-pixel grid and averaging. Interleaving is viable because the offsets used are small, $< 10''$.

Depth is built up by averaging several Leavstack frames in the same field. The result is referred to in the WSA as a 'Deepleavstack' frame. To minimise systematic errors, Leavstack frames are offset from each other by larger offsets, of order $30''$. On this scale, the variation of the pixel scale across the field of view becomes relevant, and it is necessary to re-sample the Leavstack frames for accurate registration before averaging.

For both the DXS and UDS, catalogues of sources are produced for all Leavstack and Deepleavstack frames, and are added to the respective detection tables, i.e. there can be multiple detections of a particular source in the same filter. The source tables, however, are limited to objects detected in Deepleavstack frames only. For the DXS, the EDR database contains data for fields observed in both J and K, while the EDR+ database additionally contains data where observations in only one filter have been completed. Since the UDS comprises a single Tile, querying the EDR and EDR+ databases for the UDS produces the same result.

9.2.1 DXS coverage and depth

The coverage of the DXS fields in J and K is illustrated in Figures 13 and 14, respectively. The grey-scale represents depth, established from $t_{\rm tot}$, the total integration time at any coordinate, and scaled by $1.25\log_{10}(t_{\rm tot})$. The total areal coverage is 3.3 deg^2 in J and 8.3 deg^2 in K. Figure 15 also gives a graphical representation of the DXS coverage by plotting the area that attains a given minimum depth as a function of that minimum depth. Deepleavstack frames have been created only in the fields with the largest total integration times. The stacking algorithm is similar to that used for creating the Leavstack frames. The fields are the 3 tiles (2.3 deg^2) in J and 5 tiles (3.9 deg^2) in K marked 'deep' in the coverage maps. Details of the 32 DXS Deepleavstack multiframes are provided in Table 8. The first column provides the field name, and the second is a code identifying the sub-field, in the form *Tile.XY*, where *XY* are coordinates specifying one of four multiframe positions that make up a Tile. The remaining columns give coordinates, filter, total integration time $t_{\rm tot}$, and 5σ depth.

Caveats

At the present time, we are aware of two problems affecting the DXS Leavstack and Deepleavstack frames, both related to the treatment of the noise in the sky.
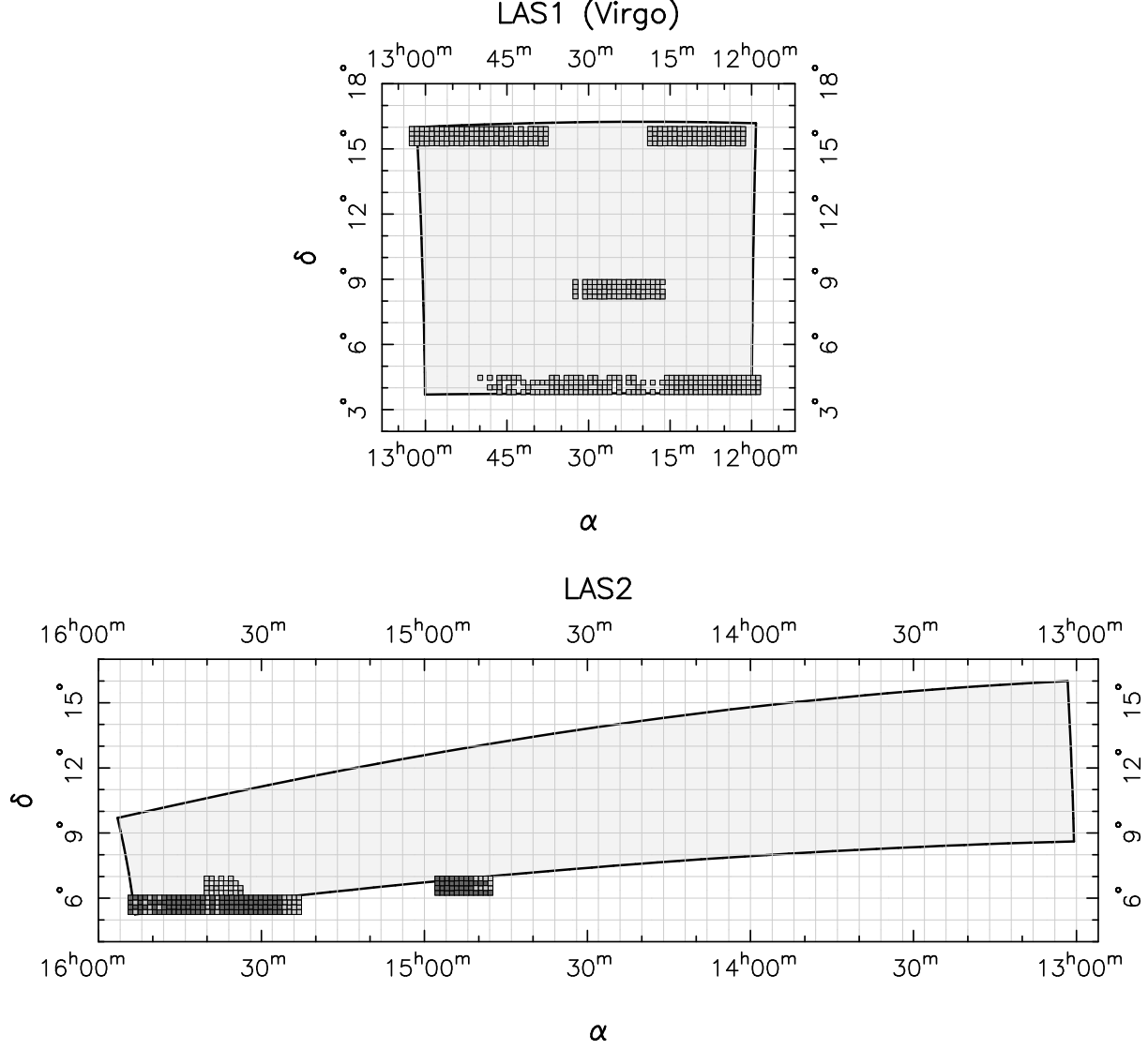
Figure 9. LAS data coverage in the EDR database (all of $YJHK$; dark grey tiles only) and the EDR+ database (all tiles), for projects LAS1 and LAS2. Each small square is a detector frame.

The stacking algorithm that produces the Leavstack frames has a default minimum value of the sky noise of 2.5 counts, which is a safety feature. In a small number of J band Leavstack frames the true value is lower. The consequence is that these frames are incorrectly weighted in forming the Deepleavstack frame, so the combination is not optimal, and the frame is not as deep as it should be. The Deepleavstack frames affected are the first four listed in Table 9.

The second problem is that the stacking and object detection algorithms operate in integer format. This has the consequence that in the deepest J band Deepleavstack frames, the sky noise is under-sampled, meaning that there is a digitisation noise contribution. The result is that the sky noise is greater than it need be, and so the detection limits are not as deep as they should be.

Both problems will be remedied in DR1.

9.2.2 UDS coverage and depth

The UDS covers a single Tile and so is not illustrated. The total integration times and depths reached in J and K are summarised in Table 9, where the area covered has been divided into quadrants (as explained below).

Instead of using the WFCAM pipeline software, the UDS Leavstacks were combined using TERAPIX's SWarp package (Bertin et al. 2002), with a lanczos3 kernel. The UDS Leavstacks were first mosaiced together to make single whole-Tile frames. Since the UDS data are Microstepped to 1/3 of a WFCAM pixel, the final J and K interleaved and stacked Tiles are $\sim 24000 \times 24000$ pixels, occupying some 3 Gb each on disk. To ease handling, these have been divided into four quarters. In the WSA, these quarters are referred to as 'Mosaicdeepleavstack' frames. Unlike all other stacked data in the WSA, astrometry of the deep UDS stacks uses tangential projection (TAN) rather than the zenith polynomial projection (ZPN) that is standard for WFCAM.
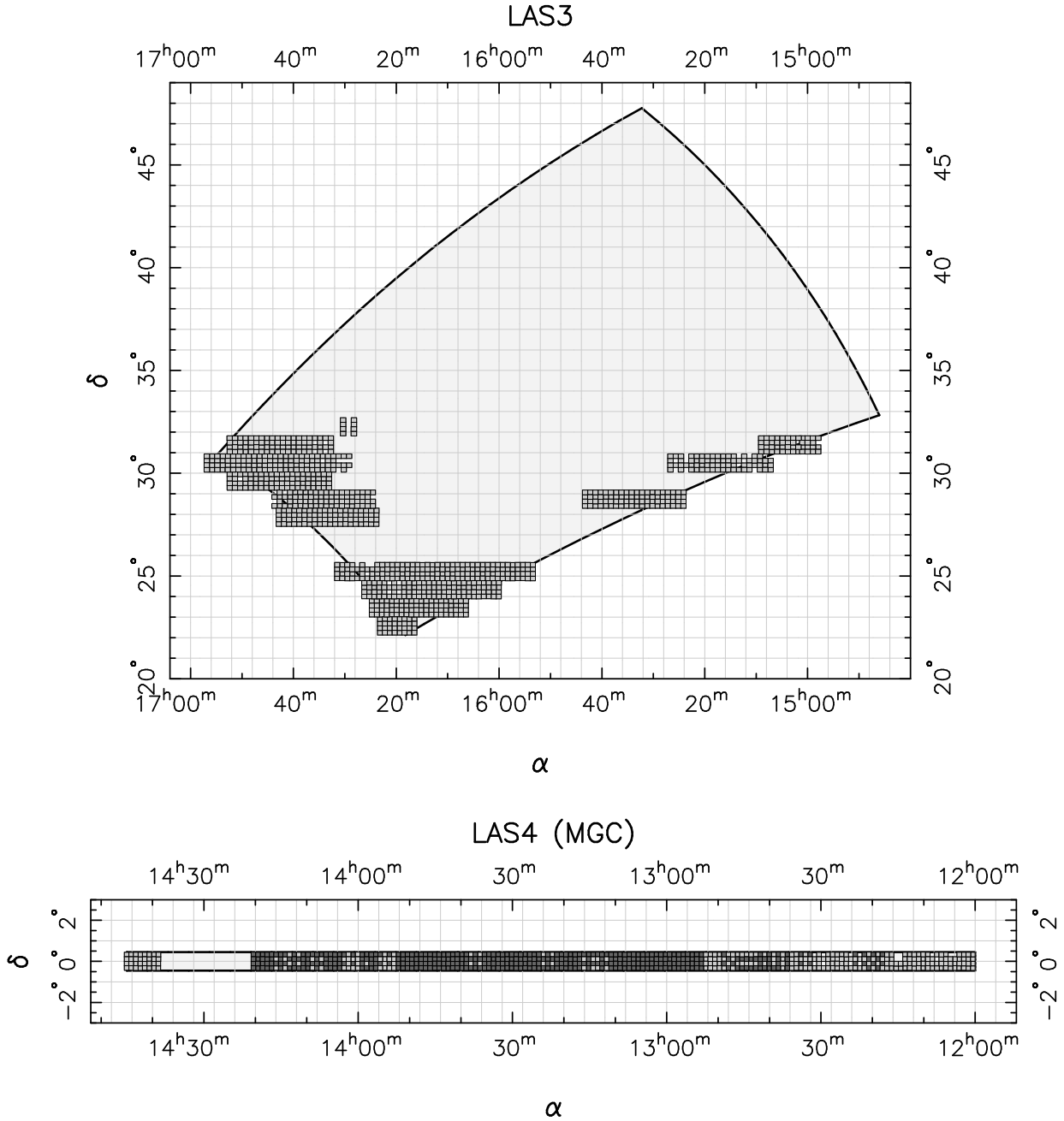
Figure 10. LAS data coverage in the EDR database (all of $YJHK$; dark grey tiles only) and the EDR+ database (all tiles), for projects LAS3 and LAS4. LAS3 is currently only observed in J. Each small square is a detector frame.

Caveats

The source detection algorithm used to generate object catalogues is not optimal for the oversampled data generated by the 3×3 UDS Microstepping strategy. The result is that bright sources tend to be split into multiple sources around the edges. This problem will be rectified in DR1.

10   THE WFCAM SCIENCE ARCHIVE

In this section we outline the architecture of the WSA in its current state, and describe the principal means by which users can access the data. The WSA will continue to develop over the course of the 2-year plan. Upgrades of the WSA will be announced in future data releases as they occur. We refer the reader to Hambly et al. (2006) for more information.

10.1   WSA architecture

Pipeline-processed images and catalogues are held in the WSA, hosted in Edinburgh by WFAU. Image data are stored in the same MEF format produced by the pipeline, with a primary header and one header per extension. The MEF files are the *multiframes* referred to previously. The object data from the individual catalogues are extracted upon ingest and
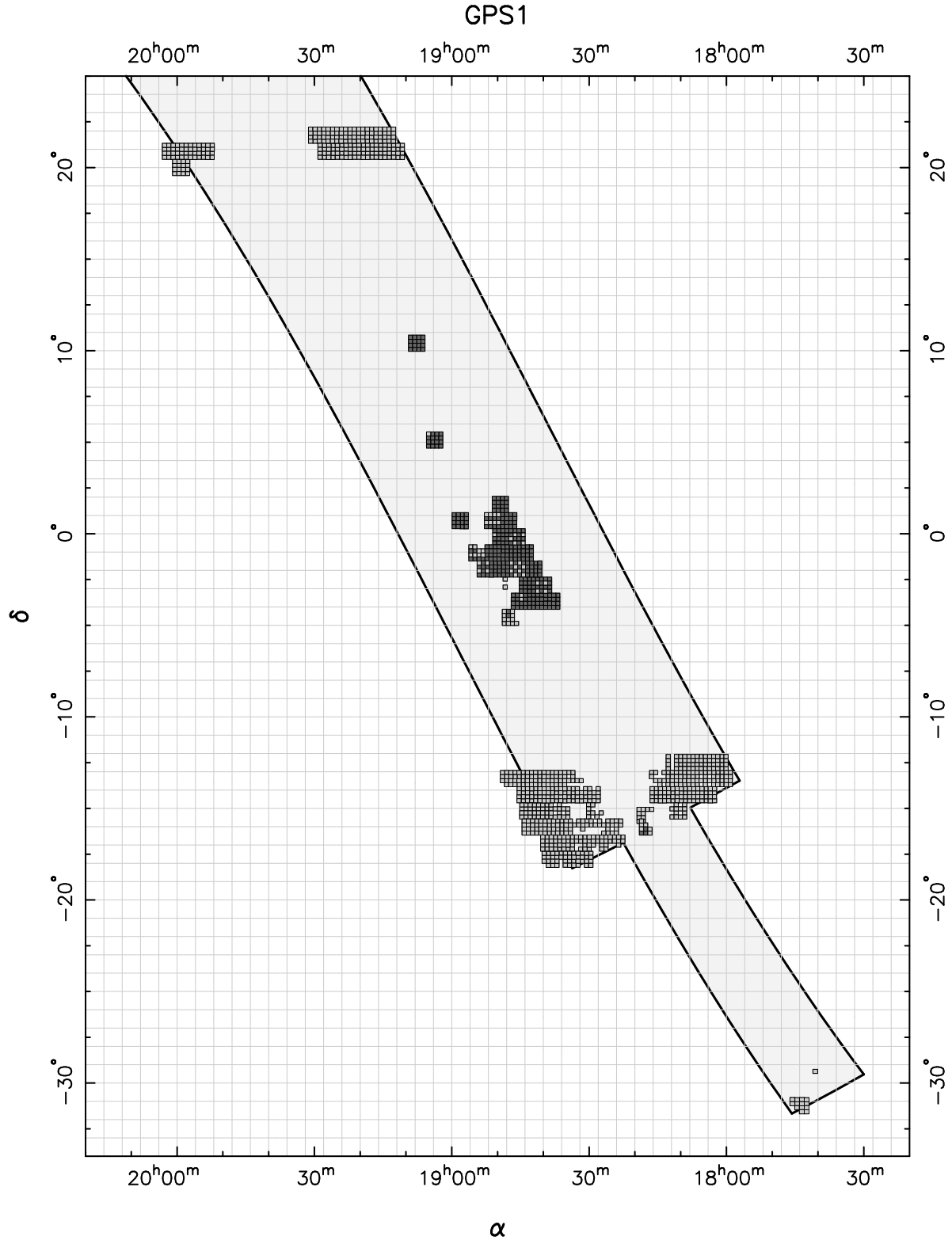
Figure 11. GPS coverage in the EDR database (all of JHK; dark grey tiles) and the EDR+ database (all tiles). EDR database coverage is specifically limited to $|b| < 1°$, $-2° < l < 107°$, and $|b| < 5°$, $30° < l < 45°$. Areas outside this are K-band only, first-epoch observations. Each small square is a detector frame.
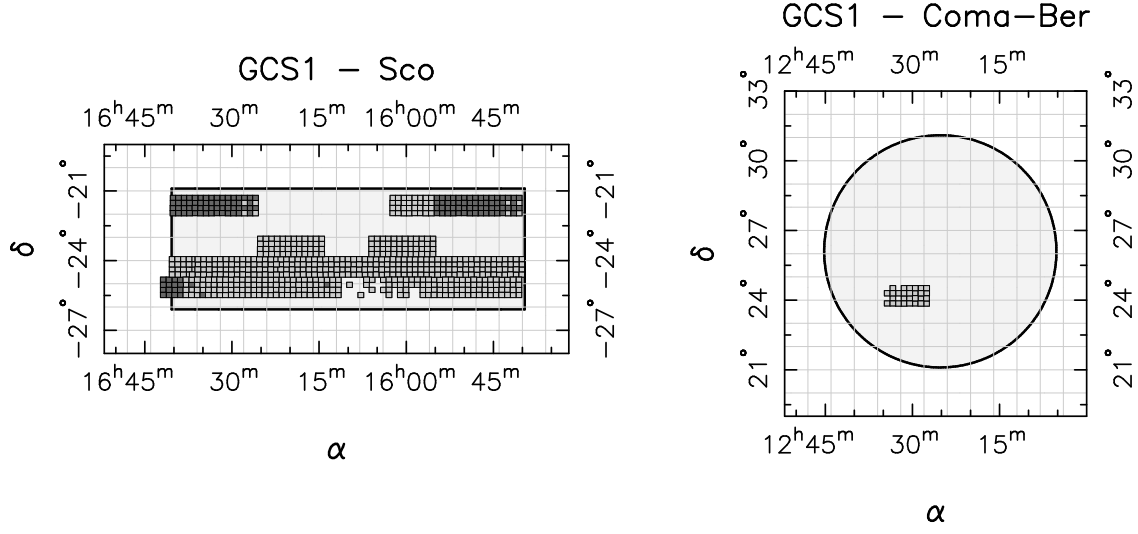
Figure 12. GCS coverage in the EDR database (all of $ZYJHK$; dark grey tiles) and the EDR+ database (all tiles). Each small square is a detector frame.

Field	Sub-field	RA (J2000)	Dec(J2000)	Filter	t_{tot} (s)	Depth (mag)
ELAIS N1[†]	1.00	242.5994000	54.5031333	J	2640.	21.42
ELAIS N1[†]	1.10	242.5994000	54.7233250	J	4420.	21.64
ELAIS N1[†]	1.01	242.9817370	54.5031333	J	6060.	21.69
ELAIS N1[†]	1.11	242.9817370	54.7233250	J	5060.	21.62
ELAIS N1	1.00	242.5994000	54.5031333	K	4500.	20.43
ELAIS N1	1.10	242.5994000	54.7233250	K	4500.	20.51
ELAIS N1	1.01	242.9817370	54.5031333	K	5000.	20.53
ELAIS N1	1.11	242.9817370	54.7233250	K	3500.	20.33
Lockman Hole	1.00	163.3623000	57.4753556	K	3500.	20.35
Lockman Hole	1.10	163.3623000	57.6955472	K	2500.	20.19
Lockman Hole	1.01	163.7756167	57.4753556	K	2000.	20.19
Lockman Hole	1.11	163.7756167	57.6955472	K	2000.	20.02
XMM-LSS	1.00	36.5752020	-4.7496444	J	5760.	22.26
XMM-LSS	1.10	36.5803542	-4.5294528	J	6400.	22.28
XMM-LSS	1.01	36.8012000	-4.7496444	J	5760.	22.24
XMM-LSS	1.11	36.8012000	-4.5294528	J	5760.	22.27
XMM-LSS	1.00	36.5752020	-4.7496444	K	6400.	20.83
XMM-LSS	1.10	36.5803542	-4.5294528	K	6400.	20.87
XMM-LSS	1.01	36.8012000	-4.7496444	K	6400.	20.82
XMM-LSS	1.11	36.8012000	-4.5294528	K	3840.	20.62
VIMOS 4	1.00	334.2667458	0.1698000	J	8320.	22.21
VIMOS 4	1.10	334.2667458	0.3899917	J	10880.	22.38
VIMOS 4	1.01	334.4869458	0.1698000	J	9600.	22.36
VIMOS 4	1.11	334.4869458	0.3899917	J	5760.	22.18
VIMOS 4	1.00	334.2667458	0.1698000	K	9120.	20.82
VIMOS 4	1.10	334.2667458	0.3899917	K	12180.	21.00
VIMOS 4	1.01	334.4869458	0.1698000	K	10900.	20.95
VIMOS 4	1.11	334.4869458	0.3899917	K	9620.	20.97
VIMOS 4	2.00	335.1420250	0.1817444	K	7680.	20.90
VIMOS 4	2.10	335.1420250	0.4019361	K	8320.	20.91
VIMOS 4	2.01	335.3622250	0.1817444	K	8960.	20.92
VIMOS 4	2.11	335.3622250	0.4019361	K	8960.	20.88

Table 8. DXS Deepleavstack multiframes. The field, sub-field code, base coordinates, filter, total Integration time in seconds and 5σ point source sensitivity of each multiframe are listed. [†]These four J stacks are affected by the first sky noise problem discussed in the text.
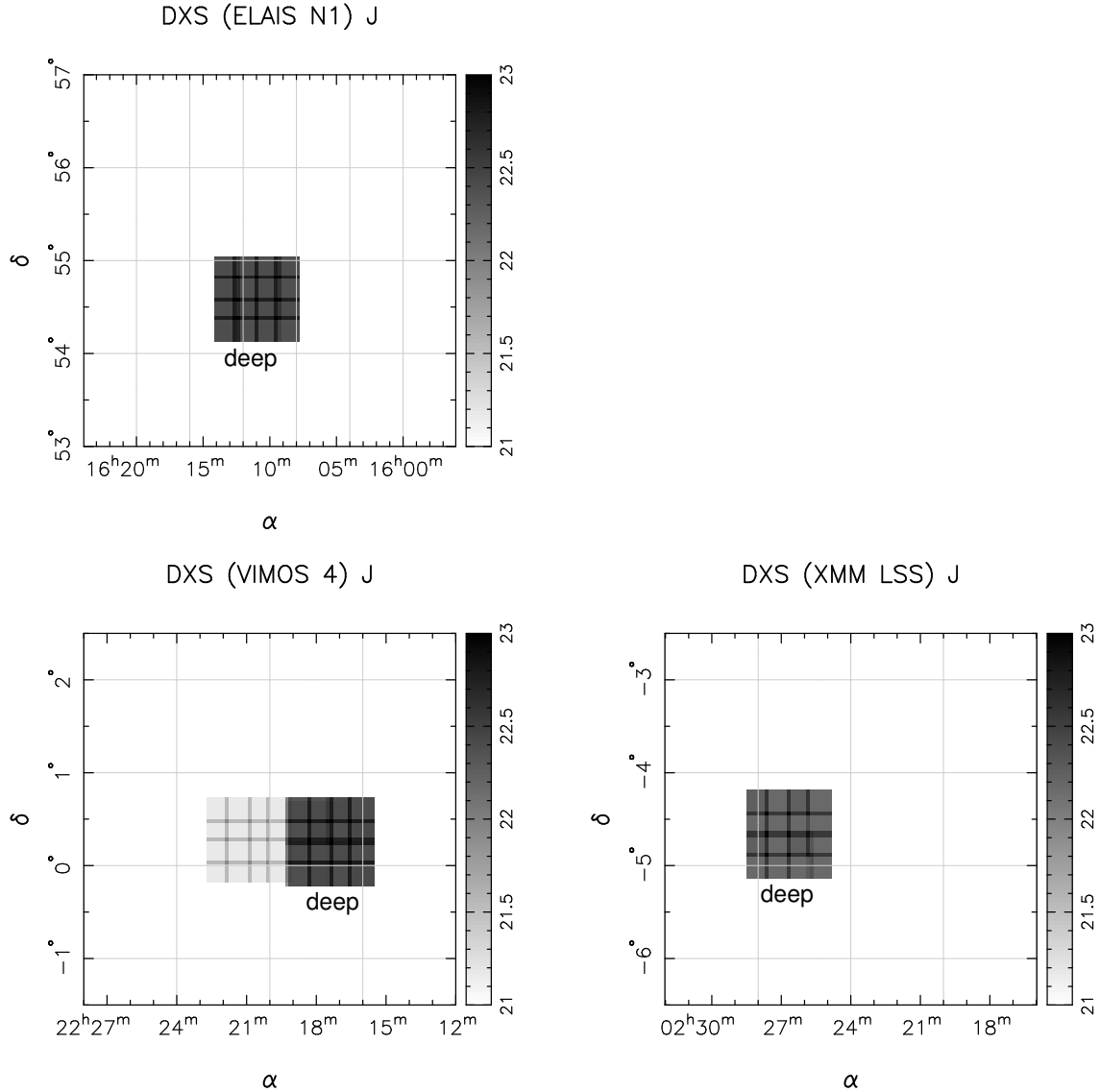
DXS (ELAIS N1) J

DXS (VIMOS 4) J

DXS (XMM LSS) J

Figure 13. DXS coverage and depth in J. Tiles that are available from the WSA as Deepleavstacks are labelled. Grey-shaded key gives depth in J.

placed in a relational database running on Microsoft SQL Server 2000. The individual catalogue files are nevertheless retained, and are stored in MEF format.

The multiframe is the principal component of the WSA. The most common multiframe corresponds to a single WF-CAM Integration. Multiframes exist for all observation types (e.g. dark, flat, object) and data products (e.g. Normal, Leav & Stack). The WSA refers to the primary header of a Multiframe as extension 1 (via the attribute `extNum` – see below). Extensions 2 to 5 correspond to the headers and pixel data for detectors 1 to 4 respectively. The primary header includes *metadata* applicable to all objects in the multiframe, such as the airmass and filter. The subsidiary headers include metadata applicable to the individual detectors, such as the average ellipticity for point sources and the astrometry coefficients. Each multiframe is assigned a unique ID number, `multiframeID`, which is an attribute in many tables held in the archive. The attribute `multiframeID` is used,

often in conjunction with the attribute `extNum`, to link the multiframe records held across tables (see Section 10.2).

All tables and their attributes are listed and described in the WSA 'schema browser'. The multiframe metadata are provided in the database in entries in three main tables. The metadata from the primary headers are held in the `Multiframe` table. Each multiframe in the archive is represented by a single row in the `Multiframe` table, with columns for attributes. The table `MultiframeDetector` contains metadata applicable to the individual detector frames of a multiframe. This excludes the astrometry calibration coefficients, which are held in the third main table, `CurrentAstrometry`. A multiframe with four extensions (detectors) gives rise to four corresponding entries (rows) in `MultiframeDetector` and `CurrentAstrometry`.

Every detection in every stack multiframe is recorded in a row in the *detection table* for the particular survey, e.g. `gpsDetection`. This means that there can be several rows
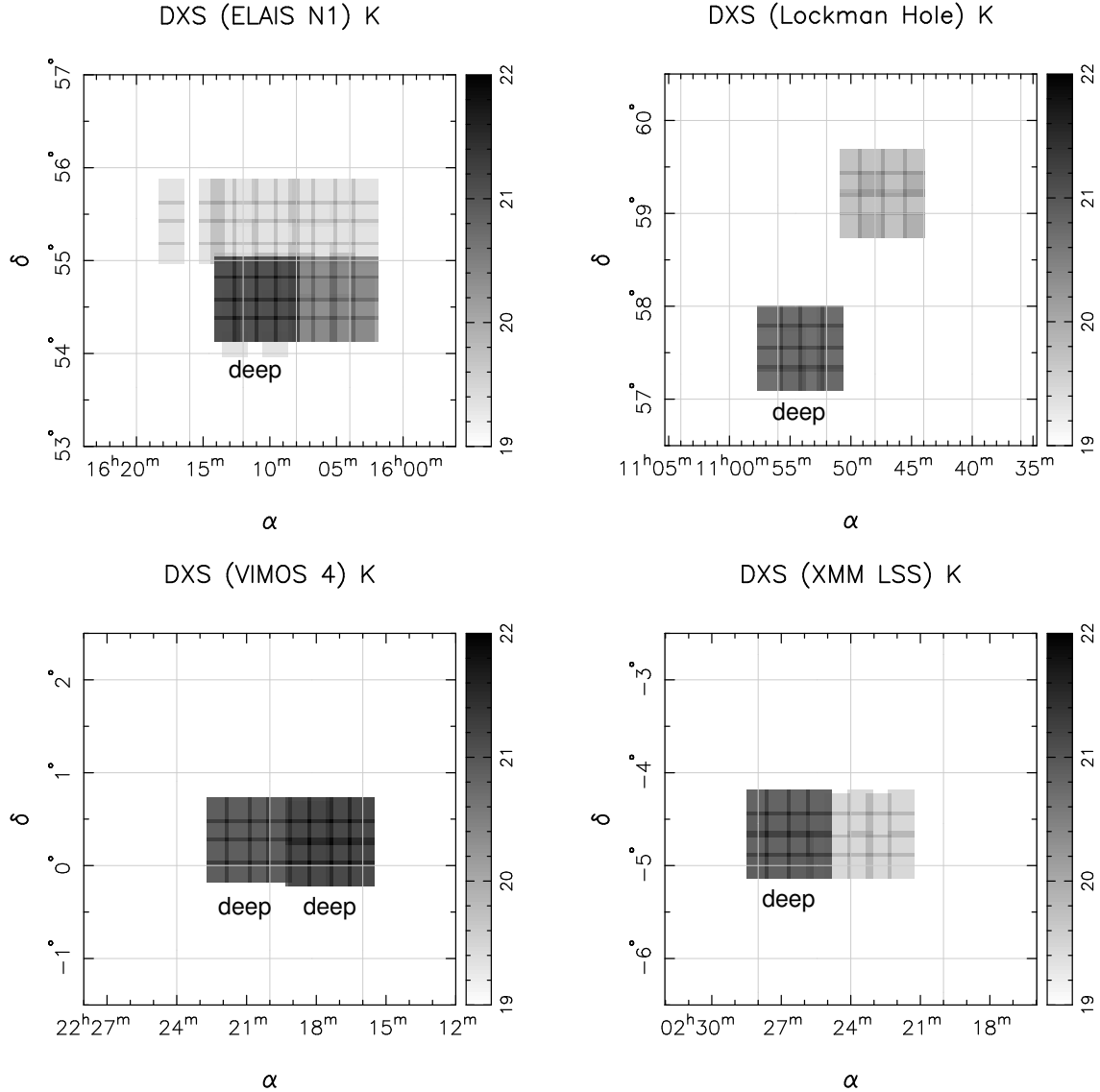
Figure 14. DXS coverage and depth in K. Tiles that are available from the WSA as Deepleavstacks are labelled. Grey-shaded key gives depth in K.

for the same object, corresponding to detections in different filters, or multiple observations in the same filter. All survey detection tables contain the same attributes. A list of the attributes is provided in Table A1. The *source table* for each survey (e.g. `gpsSource`) summarises the data in the corresponding detection table by a single row for every object, listing details of every detection of that object. Matching of multiple detections is achieved on the basis of positional coincidence. The details of the source matching algorithm are provided in Hambly et al. (2006). The number of attributes recorded in the source table, for each detection, is a subset of the attributes recorded in the detection table, to keep the number of columns in the source table manageable. The same subset is used for detections in the source tables of all the surveys. However, the number of possible detections of an object depends on the filter coverage, and number of repeat passes (Table 1), and so is different for each survey. (Note that photometry in the same filter, at

different epochs, is distinguished by e.g. `j_1`, `j_2`, for the two J epochs of the LAS.) Table A2 provides the list of attributes in the table `lasSource`. A log of the source merging is recorded in a table for each survey e.g. `lasMergeLog`. The attributes `multiframeID`, `frameSetID` and `SeqNum` are provided in the source tables to allow cross-referencing. In this way, for a particular object in a source table, it is possible to recover the full set of attributes in the detection table, for each detection. Examples of how to cross reference are provided in Section 10.2.

10.2 WSA access

The WSA is accessed at the URL `http://surveys.roe.ac.uk/wsa`. For a period of eighteen months from the release date, access to UKIDSS data is restricted to astronomers residing in ESO-member countries. For the EDR this release date was 10th February

Quadrant	RA (J2000)	Dec(J2000)	Filter	$t_{\rm tot}$ (s)	Depth
North East	34.7149375	-4.7893583	J	3160.	22.47
North West	34.2424791	-4.7893583	J	3160.	22.28
South East	34.7151208	-5.2923027	J	3160.	22.25
South West	34.2422958	-5.2923027	J	3160.	22.26
North East	34.7149375	-4.7893583	K	5240.	21.11
North West	34.2424791	-4.7893583	K	5240.	21.01
South East	34.7151208	-5.2923027	K	5240.	21.00
South West	34.2422958	-5.2923027	K	5240.	21.10

Table 9. UDS deep stacks. The centre coordinates, filter, total Integration time in seconds and 5σ point source sensitivity of each quadrant are listed.
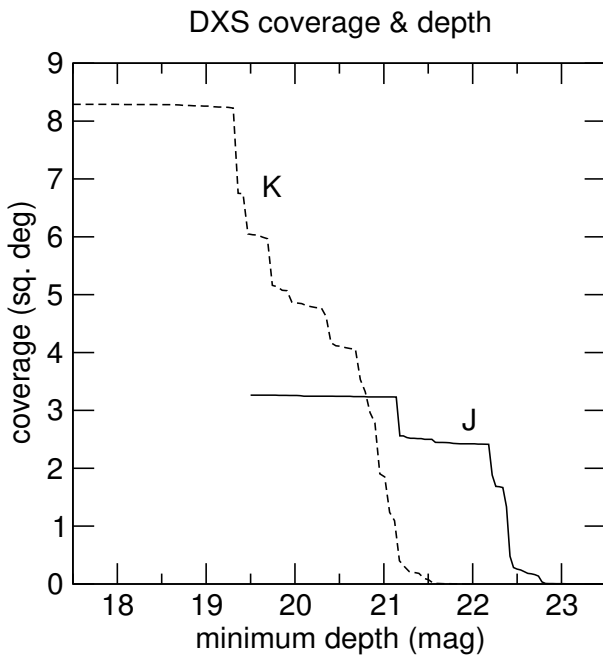

Figure 15. DXS areal coverage attaining a given minimum depth as a function of that minimum depth, for J and K.

2006. Once this restricted period has expired, the data are freely available worldwide. Access to UKIDSS data during the restricted period requires registering for an account, organised through "community contacts" at local institutions. The registration process is described on the UKIDSS web pages.[5]

10.2.1   Access to pixel data

Pixel data are obtained from the WSA using menu driven interfaces. Users can obtain details of all multiframes within an area of sky through the 'Archive Listing' interface, selecting on database (EDR or EDR+), survey, observation type (e.g. dark, flat, object), frame type (e.g. normal, leav, stack), filter and observation date. The result of a query is a table of multiframes that satisfy these criteria, with their attributes. Links are provided for each multiframe to a jpeg preview image, to the (compressed) MEF image file itself, and to

the catalogue of detections for that multiframe (in the case of stack frames). Alternatively the same list of multiframes could have been obtained with an appropriate free-form SQL query (explained below), and the MEF image file obtained by entering the `multiframeID` in the Archive Listing menu.

Instead of searching the archive by multiframe, it is possible to extract cut-out images, of a requested size, around a given position using the 'GetImage' and 'MultiGetImage' interfaces. Similar to the Archive Listing interface, the GetImage interface enables users to refine the search by database, survey, observation type, frame type, and filter, or to provide the `multiframeID`. At present, the extraction region is confined by the boundaries of the detector frame in which the given position is located and therefore limited in size by the detector dimensions. However, in the future, mosaicing of adjacent multiframes will be implemented and it will be possible to extract regions as large as $90' \times 90'$ in size. The MultiGetImage interface accepts a list of RA and Dec coordinates, currently limited to a maximum of 500. Once a submitted MultiGetImage request is completed, an email is sent to the user containing a link to their results. Jpeg preview images and FITS image files are produced and presented in web page tables and a PDF file. A tar save-set of the FITS files is also generated.

10.2.2   Access to catalogue data

The power of the WSA lies in the possibility of flexibly querying the detection and source tables. Three methods of access are offered (not counting the ability to download individual multiframe detection catalogues, explained in Section 10.2.1). The first option is a simple 'Region' search where the user selects a table (detection or source) by survey. The application returns all objects in the table within the chosen radius (currently limited to $\leqslant 90'$) of the position provided. A more sophisticated search may be carried out using the 'Menu query' interface, which the user completes in stages. After selecting the relevant table, as above, the user is presented with a list of table attributes, choosing the ones to output. One then has the option of delimiting on any of the selected attributes. From here, the request may be submitted or, alternatively, the underlying SQL query generated by the menu interface may be edited directly. In the latter case, the SQL text is passed to the free-form SQL query interface for amendment.

The final option is the free-form SQL interface. This option is the most powerful, allowing users to fully exploit the archive, including the possibility of combining tables. The

---

[5] http://www.ukidss.org/archive/archive.html

WSA web pages provide a cook-book for users unfamiliar with SQL. Below we provide some simple worked examples to illustrate the possibilities.

Example 1: Return coordinates and $2''$-diameter aperture $YJHK$ photometry of objects in a 1 deg^2 rectangular region in the LAS

This is a simple search that could be undertaken with the Menu query interface described above, which illustrates the fundamentals of SQL queries. The fact that multi-filter information is needed dictates that the table `lasSource` is required. The query is achieved with the following command (note that WSA SQL is case insensitive, capitalisation here is for clarity only):

```
SELECT ra,dec,yAperMag3,j_1AperMag3,
   hAperMag3,kAperMag3
FROM lasSource
WHERE ra BETWEEN 190 AND 191
   AND dec >= -0.5 AND dec <= 0.5
```

All SQL queries start with the `SELECT` statement followed by a list of required attributes, which in this case are the coordinates and appropriate aperture magnitudes. The second part of a simple SQL select is the `FROM` statement followed by the table name. The `WHERE` clause in the example is optional and is used here to refine the search to a $1° \times 1°$ region. Note that both RA and Dec are expressed in decimal degrees and that the SQL 'ra `BETWEEN 190 AND 191`' is identical to 'ra `>= 190 AND ra <=191`'. In addition, note that this example returns duplicated objects that lie in detector overlap regions. To eliminate these, another line of SQL must be appended to select only the primary entry using the `priOrSec` attribute: `AND (priOrSec=0 OR priOrSec=frameSetID)`

As an example of the flexibility of the WSA, one could use a simple command of this type to select rare objects of unusual colour, and use the output to check the reality of the candidates using MultiGetImage. A variety of different formats for the output of a SQL query is offered. By outputting a list of RA and Dec of objects satisfying certain colour criteria, and selecting uncompressed ASCII output, the resulting file may be edited to remove the header, and then directly read by the MultiGetImage interface, to return FITS images of each candidate.

Example 2: Find all K-band detector frames in the GPS with fewer than 30000 detected objects

To achieve this, the attributes `filterID` and `tableRows` in the table `MultiframeDetector` provide the filter name and the number of objects detected.[6] However, there is no attribute in `MultiframeDetector` which can be used to identify the survey. A SQL 'join' with table `Multiframe` must be made, using the attribute `multiframeID` as the common link, in order to access the attribute `project` (a survey is divided into several projects, for administrative purposes). The following SQL provides the required result:

```
SELECT M.multiframeID,extNum
FROM MultiframeDetector AS MD, Multiframe AS M
```

---

[6] `filterID`=1 to 8 corresponds to filters Z, Y, J, H, K, H_2, $Br\gamma$, and dark respectively. The SQL '`SELECT * FROM Filter`' gives further details.

```
WHERE tableRows < 30000
   AND M.multiframeID = MD.multiframeID
   AND project LIKE "U/UKIDSS/GPS%"
   AND M.filterID=5
   AND frameType LIKE "%stack"
```

Here, both table names are relabelled with the `AS` function to simplify the SQL. To prevent ambiguities, attributes common to both tables, such as `filterID`, must be uniquely specified by prefixing them with the relevant table name, or as in the example above, its relabelled name, e.g. `M.filterID`. The join is achieved by stipulating `M.multiframeID = MD.multiframeID`. The `%` sign is a wildcard, used in conjunction with `LIKE`, to include all GPS projects, and all types of stack frame (including Stack and Leavstack).

Example 3: Return the distribution of depths reached in GCS J-band stacked detector frames

In this example, we use the definition of point-source 5σ depth given by equation (4), explained in Section 8. This formula requires the attributes `photZPCat`, `skyNoise` and `AperCor3`, respectively the photometric zero point m_0, the background noise σ_{sky}, and the aperture correction m_{ap}, from the table `MultiframeDetector`, as well as the attribute `expTime`, the exposure time t_{exp}, from the table `Multiframe`. The formula also requires the calculation of N the number of pixels in the aperture, which depends on the pixel size, given by `xPixSize` in the table `CurrentAstrometry` (recall that the pixel size is smaller in an interlaced frame). Then the number of pixels is given by $N = \pi/\text{xPixSize}^2$, for the $2''$-diameter aperture used.

Since attributes are used from the tables `MultiframeDetector`, `Multiframe`, and `CurrentAstrometry`, a three-way join is needed:

```
SELECT CAST(ROUND(T.depth*10.0,0) AS INT)/10.0
   AS depthBin, COUNT(*)
FROM (
      SELECT photZPCat
         -2.5*LOG10(5.0*skyNoise*
         SQRT(1.2*3.141593)/(xPixSize*expTime))
         -AperCor3 AS depth
      FROM MultiframeDetector AS MFD,
         Multiframe AS M,
         CurrentAstrometry AS CA
      WHERE M.multiframeID=MFD.multiframeID
         AND CA.MultiframeID=MFD.MultiframeID
         AND CA.extNum=MFD.extNum
         AND project LIKE "u/ukidss/gcs%"
         AND M.filterID=3
         AND frameType LIKE "%stack"
      ) AS T
GROUP BY CAST(ROUND(T.depth*10.0,0) AS INT)/10.0
ORDER BY depthBin
```

This is an example of a nested select. The inner select statement returns a table, labelled `T` here, which is the list of depths required. The table `T` is then subject to the external select statement. To return a distribution of depths, the above SQL does three things: 1) rounds depths to the nearest 0.1 mag with the function `CAST(ROUND(T.depth*10.0,0) AS INT)/10.0`, 2) groups these binned depths together with

the `GROUP BY` statement, 3) counts the number of binned depths in each group with `COUNT(*)`. The `ORDER BY` statement simply returns results in order of ascending bin magnitude.

For further examples and more information on access to the WSA, we refer the reader to the WSA Cookbook, Schema Browser and Data Access/Overview via the web address given at the beginning of this section (see also Hambly et al. 2006).

11   SUMMARY

The UKIDSS EDR is the first ESO-wide release of UKIDSS data. The data constitute $\sim 1\%$ of the whole of UKIDSS, and are are of similar quality to, or marginally worse than, the expected data quality in future releases. Although this is only a small fraction of what UKIDSS will deliver at the end of its 7-year plan, the EDR is already comparable to the size of 2MASS in terms of the number of photons collected.

The EDR includes data from each of the five surveys that make up UKIDSS. The smaller EDR database contains ~ 50 deg^2 of pixel and catalogue data in the regions where the full complement of filters for the particular survey is complete. In addition we have released an extended database, the EDR+, that contains all data in the EDR database plus extra data that have passed QC, but in regions where the full complement of filters is incomplete. The EDR+ database constitutes approximately 220 deg^2.

In this paper, we have described the full data-train, from acquisition to release. We have given some background information to UKIDSS and an overview of the goals of the surveys. We have provided details of the observational implementation, outlined our quality control and calibration procedures, quantified the quality of the image and catalogue data and finally given instructions and worked examples for access to the WSA.

The first large release of UKIDSS data to the ESO community, DR1, will occur in mid-2006. DR1 will contain all data observed in 05A and 05B, that pass QC. We refer the reader to the UKIDSS website (*http://www.ukidss.org*) for news and progress updates.

Acknowledgements

REFERENCES

Bertin, E., Mellier, Y., Radovich, M., Missonnier, G., Didelon, P., Morin, B., 2002, '*Astronomical Data Analysis Software and Systems XI* ', ASP Conference Proceedings, Vol. 281, p. 228. Eds. D. A. Bohlender, D. Durand, & T. H. Handley.
Casali, M., et al., 2006, submitted
Churchwell, E. B., et al., 2002, AAS, 201, 5006
Cutri, R. M., et al., 2003, Explanatory Supplement to the 2MASS All Sky Data Release, IPAC
Hambly, N. C., et al., 2006, in prep.
Hawarden, T. G., Leggett, S. K., Letawsky, M. B., Ballantyne, D. R.; Casali, M. M., 2001, MNRAS, 325, 563
Hewett, P. C., Warren, S. J., Leggett, S. K., Hodgkin, S. T., 2006, MNRAS, 367, 454
Hodgkin, S. T., et al., 2006, MNRAS, in prep.
Irwin, M. J. & Trimble, V., 1984, AJ, 89, 83
Irwin, M. J., 1985, MNRAS, 214, 575
Irwin, M. J., et al. 2006, in prep.
Lawrence, A., et al., 2006, MNRAS, submitted
Liske, J., Lemon, D. J., Driver, S. P., Cross, N. J. G., Couch, W. J., 2003, MNRAS, 344, 307
Nikolaev, S., Weinberg, M. D., Skrutskie, M. F., Cutri, R. M., Wheelock, S. L., Gizis, J. E., Howard, E. M., 2000, AJ, 120, 3340
Skrutskie, M. F., et al., 2006, AJ, 131, 1163
Stoughton, C., et al., 2002, AJ, 123, 485
Tokunaga, A. T., Simons, D. A. & Vacca, W. D., 2002, PASP, 114, 180
Ungerechts, H. & Thaddeus, P., 1987, ApJS, 63, 645
York, D. G., et al., 2000, AJ, 120, 1579

APPENDIX A: TABLES OF CONTENTS OF THE WSA

For orientation, we tabulate the attributes found in all WSA detection tables (Table A1) and, as an example since they are survey specific, the attributes in the `lasSource` table (Table A2). For more complete and up-to-date information, users should refer to the online versions of these tables found in the WSA schema browser under the web address *http://surveys.roe.ac.uk/wsa*.

Name	Unit	Description
multiframeID		Unique UD (UID) of the relevant multiframe
extNum		Extension number of the multiframe
cuEventID		UID of curation event giving rise to this record
seqNum		Running number of this detection
filterID		UID of combined filter (assigned in WSA)
isoFlux	ADU	Instrumental isophotal flux counts
isoMag	mag	Calibrated isophotal magnitude
x	pix	X coordinate of detection
xErr	pix	Error in X coordinate
y	pix	Y coordinate of detection
yErr	pix	Error in Y coordinate
gauSig	pix	RMS of axes of ellipse fit
ell		1-b/a, where a,b=semi-major,-minor axis
pa	deg	Orientation of ellipse fit to x axis
aProf[1-8]	pix	No. pixels above a series of thresholds relative to local sky
pHeight	ADU	Highest pixel value above sky
pHeightErr	ADU	Error in peak height
aperFlux[1-13]	ADU	Aperture fluxes of diameter (arcsec): 1, $\sqrt{2}$, 2, $2\sqrt{2}$, 4, $4\sqrt{2}$, 8, 10, 12, 14, 16, 20, 24
aperFlux[1-13]err	ADU	Error in aperture fluxes [1-13]
aperMag[1-13]	mag	Calibrated aperture corrected aperture magnitudes [1-13]
aperMag[1-13]err	mag	Error in calibrated aperture magnitudes [1-13]
petroRad	pix	Petrosian radius r_p, defined in Yasuda et al. 2001 AJ 112 1104
kronRad	pix	Kron radius r_k, defined in Bertin and Arnouts 1996 A&A Supp 117 393
hallRad	pix	Hall radius r_h, e.g. Hall & Mackay 1984 MNRAS 210 979
petroFlux	ADU	Petrosian flux within circular aperture to $2r_p$
petroFluxErr	ADU	Error on Petrosian flux
petroMag	mag	Calibrated magnitude from Petrosian flux
petroMagErr	mag	Error on calibrated Petrosian magnitude
kronFlux	ADU	Kron flux within circular aperture to $2r_k$
kronFluxErr	ADU	Error on Kron flux
kronMag	mag	Calibrated Kron magnitude from Kron flux
kronMagErr	mag	Error on calibrated Kron magnitude
hallFlux	ADU	Hall flux within circular aperture to $2r_h$: Alternative total flux
hallFluxErr	ADU	Error on Hall flux
hallMag	mag	Calibrated magnitude from Hall flux
hallMagErr	mag	Calibrated error on Hall magnitude
errBits		Processing warning/error bitwise flags
sky	ADU	Local interpolated sky level from background tracker
skyVar	ADU	Local estimate of variation in sky level around image
deblend		Flag for parent of deblended deconstruct (redundant; only deblended images kept)
ra	deg	Celestial Right Ascension
dec	deg	Celestial Declination
cx		Unit vector of spherical coordinate
cy		Unit vector of spherical coordinate
cz		Unit vector of spherical coordinate
htmID		HTM index (20 digits) for equatorial coordinates
l	deg	Galactic longitude
b	deg	Galactic latitude
lambda	deg	SDSS system spherical coordinate 1
eta	deg	SDSS system spherical coordinate 2
class		Flag indicating most probable morphological classification
classStat		N(0,1) stellarness-of-profile statistic
psfFlux	ADU	PSF-fitted flux (**not currently implemented**)
psfFluxErr	ADU	Error on PSF-fitted flux (**not currently implemented**)
psfMag	mag	PSF-fitted calibrated magnitude (**not currently implemented**)
psfMagErr	mag	Error on PSF-fitted calibrated magnitude (**not currently implemented**)
psfFitX	pix	PSF-fitted X coordinate (**not currently implemented**)
psfFitXerr	pix	Error on PSF-fitted X coordinate (**not currently implemented**)
psfFitY	pix	PSF-fitted Y coordinate (**not currently implemented**)
psfFitYerr	pix	Error on PSF-fitted Y coordinate (**not currently implemented**)
psfFitChi2		standard normalised variance of PSF fit (**not currently implemented**)
psfFitDof		No. degrees of freedom of PSF fit (**not currently implemented**)

Table A1. List of parameters in the WSA detection table. Note that at the present time, PSF fitted fluxes and Sersic fluxes are not implemented. WSA attributes for these fluxes currently contain default values.

Name	Unit	Description
SerFlux1D	ADU	1D Sersic flux (**not currently implemented**)
SerMag1D	mag	Calibrated 1D Sersic flux (**not currently implemented**)
SerScaleLen1D		Sersic scale length (**not currently implemented**)
SerIdx1D		Power law index (**not currently implemented**)
SerFit1DChi2		Error in 1D fit (**not currently implemented**)
SerFitNu1D		1D Sersic fit nu (**not currently implemented**)
SerFlux2D	ADU	2D Sersic flux (**not currently implemented**)
SerMag2D	mag	Calibrated 2D Sersic flux (**not currently implemented**)
SerScaleLen2D		Scale length (**not currently implemented**)
SerIdx2D		Power law index (**not currently implemented**)
SerFit2DChi2		Error in 2D fit (**not currently implemented**)
SerFitNu2D		2D Sersic fit nu (**not currently implemented**)
ppErrBits		Additional WFAU post-processing error bits (currently a place holder)
deprecated		Code for a current (=0) or deprecated (!=0) detection
objID		Unique identifier for this detection

Table A1 – *continued* List of parameters in the WSA detection table.

Name	Unit	Description
sourceID		UID of merged detection
cuEventID		UID of curation event giving rise to this record
frameSetID		UID of the set of frames that this merged source comes from
ra	Degrees	Celestial Right Ascension
dec	Degrees	Celestial Declination
sigRa	Degrees	Uncertainty in RA
sigDec	Degrees	Uncertainty in Dec
epoch	Years	Epoch of position measurement
muRa	mas/yr	Proper motion in RA direction (**not currently implemented**)
muDec	mas/yr	Proper motion in Dec direction (**not currently implemented**)
sigMuRa	mas/yr	Error on proper motion in RA direction (**not currently implemented**)
sigMuDec	mas/yr	Error on proper motion in Dec direction (**not currently implemented**)
chi2		Chi-squared value of proper motion solution (**not currently implemented**)
nFrames		No. of frames used for this proper motion measurement (**not currently implemented**)
cx		unit vector of spherical co-ordinate
cy		unit vector of spherical co-ordinate
cz		unit vector of spherical co-ordinate
htmID		HTM index, 20 digits, for co-ordinate
l	Degrees	Galactic longitude
b	Degrees	Galactic latitude
lambda	Degrees	SDSS system spherical co-ordinate 1
eta	Degrees	SDSS system spherical co-ordinate 2
priOrSec		Seam code for a unique (=0) or duplicated (!=0) source (i.e. overlap duplicates)
ymj_1Pnt	mag	Point source colour Y-J
ymj_1PntErr	mag	Error on point source colour Y-J
j_1mhPnt	mag	Point source colour J-H
j_1mhPntErr	mag	Error on colour J-H
hmkPnt	mag	Point source colour H-K
hmkPntErr	mag	Error on point source colour H-K
ymj_1Ext	mag	Extended source colour Y-J
ymj_1ExtErr	mag	Error on extended source colour Y-J
j_1mhExt	mag	Extended source colour J-H
j_1mhExtErr	mag	Error on extended source colour J-H
hmkExt	mag	Extended source colour H-K
hmkExtErr	mag	Error on extended source colour H-K
mergedClassStat		Merged N(0,1) stellarness-of-profile statistic
mergedClass		Class $(1|0| - 1| - 2| - 3| - 9$=galaxy|noise|stellar|probableStar|probableGalaxy|saturated)
pStar		Probability that the source is a star
pGalaxy		Probability that the source is a galaxy
pNoise		Probability that the source is noise
pSaturated		Probability that the source is saturated
yHallMag	mag	Point source Y mag
yHallMagErr	mag	Error in point source Y mag
yPetroMag	mag	Extended source Y mag (Petrosian)
yPetroMagErr	mag	Error in extended source Y mag (Petrosian)
yPsfMag real	mag	Point source profile-fitted Y mag (**not currently implemented**)
yPsfMagErr	mag	Error in point source profile-fitted Y mag (**not currently implemented**)
ySerMag2D	mag	Extended source Y mag (profile-fitted) (**not currently implemented**)
ySerMag2DErr	mag	Error in extended source Y mag (profile-fitted) (**not currently implemented**)
yAperMag3	mag	Extended source Y mag (2.0 arcsec aperture diameter)
yAperMag3Err	mag	Error in extended source Y mag (2.0 arcsec aperture diameter)
yAperMag4	mag	Extended source Y mag (2.8 arcsec aperture diameter)
yAperMag4Err	mag	Error in extended source Y mag (2.8 arcsec aperture diameter)
yAperMag6	mag	Extended source Y mag (5.7 arcsec aperture diameter)
yAperMag6Err	mag	Error in extended source Y mag (5.7 arcsec aperture diameter)
yGausig	pixels	RMS of axes of ellipse fit in Y
yEll		1-b/a, where a/b=semi-major/minor axes in Y
yPA	Degrees	Ellipse fit celestial orientation in Y
yErrBits		Processing warning/error bitwise flags in Y
yDeblend		Flag indicating parent/child relation in Y

Table A2. List of parameters in the LAS source table. Note that attributes yHallMag to yEta repeat for each of j_1, j_2, h & k – these are omitted here for brevity. Currently, all attributes relating to proper motion and profile fitting contain default values.

Name	Unit	Description
yClass		Discrete image classification flag in Y
yClassStat		N(0,1) stellarness-of-profile statistic in Y
yppErrBits		Additional WFAU post-processing error bits in Y
ySeqNum		Running number of the Y detection
yObjID		UID of the Y detection
yXi	arcsec	Offset of Y detection from master position (+east/-west)
yEta	arcsec	Offset of Y detection from master position (+north/-south)

Table A2 – *continued* List of parameters in the LAS source table.